

# Optimal Spatial-Temporal Triangulation for Bearing-Only Cooperative Motion Estimation

Canlun Zheng<sup>a,b</sup>, Yize Mi<sup>b</sup>, Hanqing Guo<sup>b</sup>, Huaben Chen<sup>b</sup>,  
Zhiyun Lin<sup>c</sup>, Shiyu Zhao<sup>b</sup>

<sup>a</sup>College of Computer Science and Technology, Zhejiang University, Hangzhou, China.

<sup>b</sup>School of Engineering, Westlake University, Hangzhou, China.

<sup>c</sup>School of Systems Design and Intelligent Manufacturing, Southern University of Science and Technology, Shenzhen, China.

---

## Abstract

Vision-based cooperative motion estimation is an important problem for many multi-robot systems such as cooperative aerial target pursuit. This problem can be formulated as *bearing-only* cooperative motion estimation, where the visual measurement is modeled as a bearing vector pointing from the camera to the target. The conventional approaches for bearing-only cooperative estimation are mainly based on the framework distributed Kalman filtering (DKF). In this paper, we propose a new optimal bearing-only cooperative estimation algorithm, named spatial-temporal triangulation, based on the method of distributed recursive least squares, which provides a more flexible framework for designing distributed estimators than DKF. The design of the algorithm fully incorporates all the available information and the specific triangulation geometric constraint. As a result, the algorithm has superior estimation performance than the state-of-the-art DKF algorithms in terms of both accuracy and convergence speed as verified by numerical simulation. We rigorously prove the exponential convergence of the proposed algorithm. Moreover, to verify the effectiveness of the proposed algorithm under practical challenging conditions, we develop a vision-based cooperative aerial target pursuit system, which is the first of such fully autonomous systems so far to the best of our knowledge.

*Key words:* Cooperative estimation; bearing-only measurements; distributed Kalman filtering; distributed recursive least-squares; vision-based aerial target pursuit.

---

## 1 Introduction

The study in this paper is motivated by the practical task of vision-based cooperative aerial target pursuit, where multiple micro aerial vehicles (MAVs) use their onboard cameras to detect, localize, and follow an uncooperative target MAV autonomously. This task is inspired by the fascinating bird-catching-bird behaviors in nature [1]. While our previous study has considered the one-to-one case [2], the present work focus on the multiple-to-one case where multiple pursuer MAVs col-

laborate to pursuit one target MAV. The merit of using multiple pursuer MAVs is that the collaboration among the multiple pursuer MAVs can greatly enhance the target's localization performance and pursuit success rate.

Vision-based cooperative aerial target pursuit is a complex system that involves a number of interconnected components such as vision detection, motion estimation, and cooperative control.

Although there exist studies on cooperative target pursuit [3, 4] or pursuit-and-evasion problems [5, 6], these studies mainly consider control strategies by assuming that the target's motion can be obtained in other ways. Estimating the target's motion is a nontrivial problem. It is critical to accurately estimate the position and velocity of the target to achieve high-performance autonomous target pursuit.

Vision-based cooperative motion estimation can be for-

---

\* This paper was not presented at any IFAC meeting. Corresponding author: S. Zhao.

Email addresses: zhengcanlun@westlake.edu.cn (Canlun Zheng), miyize@westlake.edu.cn (Yize Mi), guohanqing@westlake.edu.cn (Hanqing Guo), chenhuaben@westlake.edu.cn (Huaben Chen), linzy@sustech.edu.cn (Zhiyun Lin), zhaoshiyu@westlake.edu.cn (Shiyu Zhao).

mulated as the problem of *bearing-only* cooperative motion estimation, where the visual measurement of a pursuer is modeled as a *bearing vector* pointing from the pursuer to the target. Specifically, when the target has been detected by certain vision algorithms, the bearing vector can be calculated from the target's pixel coordinate and the intrinsic parameters of the camera [2, 7]. By contrast, the range of the target cannot be directly recovered from a single image since the target is uncooperative and hence its prior information is unknown. It is, therefore, necessary to study how to estimate the target motion based merely on bearing measurements obtained from multiple views/images. Bearing-only motion estimation using a single moving observer has been studied extensively (see for example [2, 8, 9] and the references therein). In this paper, we focus on the case of cooperative estimation using multiple observers.

The conventional approaches for bearing-only cooperative estimation are mainly based on the framework distributed Kalman filters (DKFs) [10–13]. The state-of-the-art DKFs mainly include consensus on measurements Kalman filter (CMKF) [14], consensus on information Kalman filter (CIKF) [15, 16], and hybrid consensus on measurements and information Kalman filter (HCMCI-KF) [17]. However, the DKF-based approaches have a number of *limitations*. First, DKFs are designed for linear systems but the bearing-only estimation problem is nonlinear. As a result, the estimators designed based on linearized models becomes sub-optimal and the convergence of the entire networked system becomes difficult to analyze. Second, DKFs are designed for general systems and do not consider the unique features of bearing measurements. It is important to fully exploit bearing measurements to further improve the estimation performance. Moreover, the existing approaches mainly consider the two-dimensional case [10, 13]. Although the three-dimensional case has been studied in a few works [11, 12], the formulation based on azimuth and elevation angle measurements usually lead to complex algorithms. In addition, the target's position can also be obtained by simple triangulation [18]. However, such a method can only estimate the position of the target at a single moment and cannot give smooth estimation.

In this paper, we adopt the framework of distributed recursive least squares (DRLS) [19, 20] rather than DKF to design bearing-only cooperative estimators. DRLS provides a general and flexible way to design distributed estimation algorithms. It has some *advantages* compared to DKFs. First, DRLS is more flexible because we have the freedom to customize the objective function. As a result, we can fully utilize the available information and in the meantime balance different performance metrics. The performance of the resulting algorithm can achieve better and more explainable performance if the objective function can be well-designed. Second, a DRLS estimator requires less information shared among the pursuers to reduce the communication burden in distributed net-

works. This feature is important for inter-MAV systems where the wireless communication may have low bandwidth. Third, the convergence of a DRLS estimator can be guaranteed if the objective function is well designed with appropriate structures and coefficients. Theoretical convergence guarantee is important for cooperative bearing-only estimation, which is a nonlinear and complex networked dynamic problem.

However, applying DRLS also faces some challenges. The first challenge is that the existing DRLS algorithms mainly focus on the estimation of constant values rather than time-varying states [20–22]. Therefore, it is necessary to design new objective functions and derive DRLS estimators from scratch. The second challenge is that the convergence of DRLS algorithms is usually very complex to analyze [20]. It is even more challenging for bearing-only cooperative estimation due to its unique bearing-only feature. The structure and the coefficients of the objective function must be carefully designed to ensure estimation convergence.

In this paper, we propose a novel bearing-only cooperative estimator based on the framework of DRLS, and then apply the proposed estimator to demonstrate a real-world vision-based aerial target pursuit system. The novelties of this work are summarized as follows.

First, we design a new objective function and derive the corresponding recursive estimation algorithm called *spatial-temporal triangulation* (STT). The design of the objective function fully exploits the specific geometry and dynamic constraints of bearing-only cooperative estimation. The dynamic model is also incorporated in the objective function to ensure smooth estimation. Simulation results verify that the proposed STT algorithm has superior performance than the existing DKF algorithms in terms of both accuracy and convergence speed. It also achieves comparable performance as the centralized Kalman filter (CKF), which is usually used as a baseline to evaluate distributed estimators.

Second, we rigorously prove the exponential convergence of the STT algorithm based on carefully designed coefficients in estimator. It is important to establish the theoretical guarantee in order to obtain reliable practical applications. One key technical challenge for the convergence analysis is that the measurement matrix that corresponds to each bearing measurement is rank deficient. We fully exploit the unique features of an orthogonal projection operator (e.g., Lemma 3 to Lemma 4) that is widely used in bearing-based estimation and control tasks [2, 23], and successfully prove that the expectation of the estimation error converges exponentially fast.

Third, we develop an autonomous vision-based cooperative aerial target pursuit system to verify the effectiveness of the STT algorithm under practical challenging conditions. To the best of our knowledge, this system is

also the first autonomous vision-based cooperative aerial target pursuit system that has been ever demonstrated up to now. This system consists of three quadcopter MAVs as the pursers and one quadcopter MAV as the target. All necessary functions including visual detection, motion estimation, and formation control are realized in onboard computers. The three purser MAVs can autonomously detect the target MAV in the images by a well trained Yolo-based detector, estimate the target's position and velocity by the proposed STT algorithm, and follow the moving target to maintain a pre-specified geometric formation.

## 2 Problem Setup and Preliminaries

### 2.1 Problem statement

Consider  $n$  observers in the three-dimensional space. Each observer can obtain a noisy bearing measurement of the target by visual sensing. The observers can share information with each other over a wireless communication network. Suppose the current time step is  $k$  ( $k = 1, 2, \dots$ ). The network at time  $k$  is described by a undirected graph  $\mathcal{G}_k = \{\mathcal{V}, \mathcal{E}_k\}$ , where  $\mathcal{V} = \{1, \dots, n\}$  is the vertex set and  $\mathcal{E}_k \subseteq \mathcal{V} \times \mathcal{V}$  is the edge set. The edge  $(i, j) \in \mathcal{E}_k$  indicates that observer  $i$  can receive information from observer  $j$ , and hence the  $j$ th observer is a neighbor of the  $i$ th observer at time  $k$ . The set of neighbors of  $i$  is denoted as  $\mathcal{N}_{i,k} = \{j \in \mathcal{V} : (i, j) \in \mathcal{E}_k\}$ . The graph  $\mathcal{G}_k$  may be time-varying because wireless communication may be unreliable in practice. It is assumed that  $\mathcal{G}_k$  is always connected. That is each observer must have at least one neighbor at each time.

Suppose  $\mathbf{p}_k, \mathbf{v}_k \in \mathbb{R}^3$  are the true position and velocity of the target. Let  $\mathbf{s}_{i,k} \in \mathbb{R}^3$  be the true position of the  $i$ th observer where  $i \in \mathcal{V}$ . The unit bearing vector pointing from  $\mathbf{s}_{i,k}$  to  $\mathbf{p}_k$  is

$$\mathbf{g}_{i,k} = \frac{\mathbf{p}_k - \mathbf{s}_{i,k}}{r_{i,k}} \in \mathbb{R}^3, \quad (1)$$

where  $r_{i,k} = \|\mathbf{p}_k - \mathbf{s}_{i,k}\|$ . The noisy measurement of  $\mathbf{g}_{i,k}$  is

$$\tilde{\mathbf{g}}_{i,k} = \mathbf{R}_{i,k} \mathbf{g}_{i,k}, \quad (2)$$

where  $\mathbf{R}_{i,k}$  is a rotation matrix that perturbs  $\mathbf{g}_{i,k}$ . In particular,  $\mathbf{R}_{i,k}$  is a random rotation about a rotation axis by a small random angle. Here, the rotation axis can be any random unit vector that is orthogonal to  $\mathbf{g}_{i,k}$ .

The problem to be solved in this paper is stated as follows. Suppose the  $i$ th observer 1) knows its own position  $\mathbf{s}_{i,k}$  precisely by, for example, RTK GPS, 2) can obtain a noisy bearing measurement  $\tilde{\mathbf{g}}_{i,k}$  of the target, and 3) certain necessary information transmitted from its neigh-

bors. The aim is to estimate the target's position  $\mathbf{p}_k$  and velocity  $\mathbf{v}_k$  accurately and promptly.

### 2.2 Preliminaries: State and measurement equations

To estimate the target's motion, we first present the state transition and measurement equations.

First, the state vector of the target is defined as

$$\mathbf{x}_k = \begin{bmatrix} \mathbf{p}_k \\ \mathbf{v}_k \end{bmatrix} \in \mathbb{R}^6.$$

Suppose the state is governed by a noise-driven double-integrator model:

$$\mathbf{x}_{k+1} = \mathbf{A} \mathbf{x}_k + \mathbf{B} \mathbf{w}_k, \quad (3)$$

where

$$\mathbf{A} = \begin{bmatrix} \mathbf{I}_{3 \times 3} & \Delta t \mathbf{I}_{3 \times 3} \\ \mathbf{0}_{3 \times 3} & \mathbf{I}_{3 \times 3} \end{bmatrix} \in \mathbb{R}^{6 \times 6}, \quad (4)$$

$$\mathbf{B} = \begin{bmatrix} \mathbf{0}_{3 \times 3} \\ \mathbf{I}_{3 \times 3} \end{bmatrix} \in \mathbb{R}^{6 \times 3}.$$

Here,  $\mathbf{w}_k \in \mathbb{R}^3$  is a zero-mean Gaussian noise:  $\mathbf{w} \sim \mathcal{N}(0, \Sigma_{\mathbf{w}})$ , where  $\Sigma_{\mathbf{w}} = \sigma_{\mathbf{w}}^2 \mathbf{I}_{3 \times 3}$ . In addition,  $\Delta t$  is the sampling time,  $\mathbf{I}_{3 \times 3} \in \mathbb{R}^{3 \times 3}$  is the identity matrix, and  $\mathbf{0}_{3 \times 3} \in \mathbb{R}^{3 \times 3}$  is a zero matrix.

Second, we establish the measurement equation. The noisy bearing vector in (2) is a *nonlinear equation* of the target's state. It is necessary to covert it to a *pseudo-linear equation* to achieve better estimation stability [8].

To that end, we introduce a useful orthogonal projection operator that will be frequently used in this paper. For any unit vector  $\mathbf{g} \in \mathbb{R}^3$ , define

$$\mathbf{P}_{\mathbf{g}} = \mathbf{I}_{3 \times 3} - \mathbf{g} \mathbf{g}^T \in \mathbb{R}^{3 \times 3}. \quad (5)$$

The interpretation of  $\mathbf{P}_{\mathbf{g}}$  is that, for any vector  $\mathbf{z} \in \mathbb{R}^3$ , the product  $\mathbf{P}_{\mathbf{g}} \mathbf{z}$  is the orthogonal projection of  $\mathbf{z}$  onto the plane that is orthogonal to  $\mathbf{g}$ . It holds that  $\mathbf{P}_{\mathbf{g}} = \mathbf{P}_{\mathbf{g}}^T$ ,  $\mathbf{P}_{\mathbf{g}}^2 = \mathbf{P}_{\mathbf{g}}$ , and  $\text{Null}(\mathbf{P}_{\mathbf{g}}) = \text{span}(\mathbf{g})$ . The projection matrix  $\mathbf{P}_{\mathbf{g}}$  plays important roles in bearing-related problems [24].

With this orthogonal projection matrix, we can convert the nonlinear measurement equation (2) to be pseudo-linear. To that end, we have

$$\begin{aligned} \tilde{\mathbf{g}}_{i,k} &= \mathbf{R}_{i,k} \mathbf{g}_{i,k} \\ &= \mathbf{g}_{i,k} + \underbrace{(\mathbf{R}_{i,k} \mathbf{g}_{i,k} - \mathbf{g}_{i,k})}_{\boldsymbol{\mu}_{i,k}}. \end{aligned} \quad (6)$$

Multiplying  $\mathbf{P}_{\tilde{\mathbf{g}}_{i,k}}$  on both sides of (6) gives

$$\mathbf{0} = \mathbf{P}_{\tilde{\mathbf{g}}_{i,k}}(\mathbf{g}_{i,k} + \boldsymbol{\mu}_{i,k}),$$

where the left-hand side is zero because  $\mathbf{P}_{\tilde{\mathbf{g}}_{i,k}}\tilde{\mathbf{g}}_{i,k} = \mathbf{0}$ . Substituting the expression of  $\mathbf{g}_{i,k}$  in (1) into the above equation yields

$$\mathbf{0} = \mathbf{P}_{\tilde{\mathbf{g}}_{i,k}} \left( \frac{\mathbf{p}_k - \mathbf{s}_{i,k}}{r_{i,k}} + \boldsymbol{\mu}_{i,k} \right),$$

which can be reorganized to

$$\mathbf{P}_{\tilde{\mathbf{g}}_{i,k}} \mathbf{s}_{i,k} = \mathbf{P}_{\tilde{\mathbf{g}}_{i,k}} \mathbf{p}_k + (r_{i,k} \mathbf{P}_{\tilde{\mathbf{g}}_{i,k}} \boldsymbol{\mu}_{i,k}),$$

which can be further expressed as

$$\underbrace{\mathbf{P}_{\tilde{\mathbf{g}}_{i,k}} \mathbf{s}_{i,k}}_{\mathbf{z}_{i,k}} = \underbrace{\left[ \mathbf{P}_{\tilde{\mathbf{g}}_{i,k}} \quad \mathbf{0}_{3 \times 3} \right]}_{\mathbf{H}_{i,k}} \mathbf{x}_k + \underbrace{(r_{i,k} \mathbf{P}_{\tilde{\mathbf{g}}_{i,k}} \boldsymbol{\mu}_{i,k})}_{\boldsymbol{\nu}_{i,k}}. \quad (7)$$

Equation (7) is the pseudo-linear measurement equation. It is called pseudo-linear because, although the expression is linear in the state  $\mathbf{x}_k$ , both the state matrix  $\mathbf{H}_{i,k}$  and noise  $\boldsymbol{\nu}_{i,k}$  are functions of the measurement. Although the noise  $\boldsymbol{\nu}_{i,k}$  is not Gaussian anymore, the pseudo-linear equation can achieve better stability than the nonlinear extended Kalman filter [8].

### 2.3 Preliminaries: Some useful results

We next introduce some mathematical preliminaries that will be used throughout this paper.

Let  $\sigma_{\min}(\cdot)$  and  $\sigma_{\max}(\cdot)$  be the smallest and greatest singular values of a matrix, respectively. Denote  $\|\cdot\|$  as the spectral norm of a matrix. For any non-singular square matrix  $\mathbf{A}$ , we have  $\|\mathbf{A}\| = \sigma_{\max}(\mathbf{A})$  and  $\|\mathbf{A}^{-1}\| = 1/\sigma_{\min}(\mathbf{A})$ . If a matrix is symmetric positive semi-definite, the singular values are equal to its eigenvalues.

For any two symmetric positive semi-definite matrices  $\mathbf{A}$  and  $\mathbf{B}$ , it holds that

$$\sigma_{\min}(\mathbf{A} + \mathbf{B}) \geq \sigma_{\min}(\mathbf{A}) + \sigma_{\min}(\mathbf{B}).$$

If  $\mathbf{A} - \mathbf{B} \geq 0$ , which means  $\mathbf{A} - \mathbf{B}$  is positive semi-definite, then  $\sigma_{\min}(\mathbf{A}) \geq \sigma_{\min}(\mathbf{B})$ . Suppose  $\mathbf{A}$ ,  $\mathbf{B}$ , and  $\mathbf{C}$  are matrices with appropriate dimensions. Let  $\otimes$  be the Kronecker product. Then,

$$\mathbf{A} \otimes (\mathbf{B} + \mathbf{C}) = \mathbf{A} \otimes \mathbf{B} + \mathbf{A} \otimes \mathbf{C}.$$

Suppose  $\sigma_i(\mathbf{A})$  and  $\sigma_j(\mathbf{B})$  are the  $i$ th and  $j$ th singular values of  $\mathbf{A}$  and  $\mathbf{B}$ , respectively. Then, the set of singular

values of  $\mathbf{A} \otimes \mathbf{B}$  is  $\{\sigma_i(\mathbf{A})\sigma_j(\mathbf{B})\}_{i,j}$ . As a consequence,

$$\sigma_{\min}(\mathbf{A} \otimes \mathbf{B}) = \sigma_{\min}(\mathbf{A})\sigma_{\min}(\mathbf{B}). \quad (8)$$

Finally, if  $\mathbf{A}$ ,  $\mathbf{C}$ , and  $\mathbf{A} + \mathbf{C}$  are non-singular, then [25]

$$(\mathbf{A} + \mathbf{C})^{-1} = (\mathbf{I} - (\mathbf{C}^{-1}\mathbf{A} + \mathbf{I})^{-1})\mathbf{A}^{-1}. \quad (9)$$

## 3 Spatial-Temporal Triangulation Algorithm

This section presents and analyzes a new cooperative bearing-only target motion estimator called *spatial-temporal triangulation* (STT) based on the framework of DRLS. Here, “spatial” refers to the information obtained from multiple observers located at different spatial positions at the same moment. Here, “temporal” refers to the historical information obtained by each observer at different moments.

### 3.1 Objective function

First of all, we define an objective function that can 1) fully utilize all the information available to each observer, 2) balance different performance metrics such as estimation smoothness and convergence speed, and 3) ensure the resulting algorithm is convergent.

Suppose  $\hat{\mathbf{x}}_{i,t}$  is the estimate of the target state  $\mathbf{x}$  by observer  $i$  at time  $t$ .

First, define the *measurement error* for observer  $i$  as

$$\begin{aligned} J_{\text{pred}}(\hat{\mathbf{x}}_{i,t}) &= \sum_{j \in (i \cup \mathcal{N}_{i,t})} \alpha_{ij,t} (\mathbf{z}_{j,t} - \mathbf{H}_{j,t} \hat{\mathbf{x}}_{i,t})^T \mathbf{R} (\mathbf{z}_{j,t} - \mathbf{H}_{j,t} \hat{\mathbf{x}}_{i,t}) \\ &\doteq \sum_{j \in (i \cup \mathcal{N}_{i,t})} \|\mathbf{z}_{j,t} - \mathbf{H}_{j,t} \hat{\mathbf{x}}_{i,t}\|_{\alpha, \mathbf{R}}^2. \end{aligned}$$

The measurement error  $J_{\text{pred}}(\hat{\mathbf{x}}_{i,t})$  represents the *discrepancy between the estimates and the measurements*. More specifically, it involves  $(\mathbf{z}_{i,t} - \mathbf{H}_{i,t} \hat{\mathbf{x}}_{i,t})$  and  $(\mathbf{z}_{j,t} - \mathbf{H}_{j,t} \hat{\mathbf{x}}_{i,t})$  with  $j \in \mathcal{N}_{i,t}$ . Here,  $(\mathbf{z}_{i,t} - \mathbf{H}_{i,t} \hat{\mathbf{x}}_{i,t})$  indicates the deficiency between observer  $i$ 's measurement and estimate.  $(\mathbf{z}_{j,t} - \mathbf{H}_{j,t} \hat{\mathbf{x}}_{i,t})$  indicates the deficiency between observer  $i$ 's estimate and observer  $j$ 's measurement. Here,  $\alpha_{ij,t} \geq 0$  is a weight and satisfies  $\sum_{j \in (i \cup \mathcal{N}_{i,t})} \alpha_{ij,t} = 1$ . The weight matrix  $\mathbf{R}$  is selected as  $\mathbf{R} = \mathbf{I}_{3 \times 3} / \sigma_v^2 \in \mathbb{R}^{3 \times 3}$ . This measurement error incorporates the constraint of triangulation geometry. In the ideal case, this measurement error should be zero, meaning that the bearing measurements of different observers intersect at the same point in the 3D space and the estimate coincides with this point.

Second, define the *consensus error* as

$$\begin{aligned} J_{\text{cons}}(\hat{\mathbf{x}}_{i,t}) &= \sum_{j \in (i \cup \mathcal{N}_{i,t})} \beta_{ij,t} (\hat{\mathbf{x}}_{j,t}^- - \hat{\mathbf{x}}_{i,t})^T (\hat{\mathbf{x}}_{j,t}^- - \hat{\mathbf{x}}_{i,t}) \\ &\doteq \sum_{j \in (i \cup \mathcal{N}_{i,t})} \|\hat{\mathbf{x}}_{j,t}^- - \hat{\mathbf{x}}_{i,t}\|_{\beta}^2, \end{aligned}$$

where  $\hat{\mathbf{x}}_{j,t}^- = \mathbf{A}\hat{\mathbf{x}}_{j,t-1}$  is the predicted estimate of neighbor  $j$ . The consensus error  $J_{\text{cons}}$  represents the *deficiency between the estimates of observer  $i$  and its neighbors*. The reason that  $\hat{\mathbf{x}}_{j,t}^-$  is used rather than  $\hat{\mathbf{x}}_{j,t}$  is that the later is still unknown at time  $t$ . Here,  $\beta_{ij,t} \geq 0$  is a weight and satisfies  $\sum_{j \in (i \cup \mathcal{N}_{i,t})} \beta_{ij,t} = 1$ . In the ideal case, this consensus error should be zero, meaning that all the observers have reached a consensus on the target's state.

Both of the measurement and consensus errors are for a single time step  $t$ . The overall objective function is the sum of the two errors over the time horizon of  $t = 1, \dots, k$ :

$$J(\{\hat{\mathbf{x}}_{i,t}\}_{t=1}^k) = c \sum_{t=1}^k \lambda_t^{(k)} J_{\text{pred}}(\hat{\mathbf{x}}_{i,t}) + \sum_{t=1}^k \lambda_t^{(k)} J_{\text{cons}}(\hat{\mathbf{x}}_{i,t}), \quad (10)$$

where  $c$  is a positive weight to balance  $J_{\text{pred}}$  and  $J_{\text{cons}}$ . Here,  $\lambda_t^{(k)} \in (0, 1)$  is a *forgetting factor* that depends on both  $t$  and  $k$ . When  $\lambda_t^{(k)}$  is close to 0, less weight is given to the distant past information. When  $\lambda_t^{(k)}$  is close to 1, more weight is given to the distant past information. The design of  $\lambda_t^{(k)}$  also influence the estimation stability. The specific expression of it will be given later.

The objective function in (10) incorporates all the available information and geometric constraint in the problem of bearing-only cooperative motion estimation. Only in this way, the resulting algorithm can generate high-performance estimation. In the ideal case this objective function should be equal to zero. In practice, it is usually nonzero and we need to find the optimal estimate that can minimize it.

To that end, we further incorporate the dynamic constraints among  $\{\hat{\mathbf{x}}_{i,t}\}_{t=1}^k$ . In particular, it follows from the state transition equation that  $\hat{\mathbf{x}}_{i,t+1} = \mathbf{A}\hat{\mathbf{x}}_{i,t}$ , where  $\mathbf{A}$  is given in (4). Then, we have  $\hat{\mathbf{x}}_{i,t} = \mathbf{A}^{t-k} \hat{\mathbf{x}}_{i,k}$ , sub-

stituting which into (10) gives

$$\begin{aligned} &J(\hat{\mathbf{x}}_{i,k}) \\ &= c \sum_{t=1}^k \left( \lambda_t^{(k)} \sum_{j \in (i \cup \mathcal{N}_{i,t})} \|\mathbf{z}_{j,t} - \mathbf{H}_{j,t} \mathbf{A}^{t-k} \hat{\mathbf{x}}_{i,k}\|_{\alpha, \mathbf{R}}^2 \right) \\ &\quad + \sum_{t=1}^k \left( \lambda_t^{(k)} \sum_{j \in (i \cup \mathcal{N}_{i,t})} \|\hat{\mathbf{x}}_{j,t}^- - \mathbf{A}^{t-k} \hat{\mathbf{x}}_{i,k}\|_{\beta}^2 \right). \quad (11) \end{aligned}$$

Thus, the objective function of  $\{\hat{x}_{i,t}\}_{t=1}^k$  in (10) becomes an objective function of  $\hat{x}_{i,k}$  in (11).

### 3.2 The proposed STT algorithm

We next present the algorithm that can find the optimal solution of (11). First of all, we design the forgetting factor as

$$\lambda_t^{(k)} = \frac{\gamma_2^{k-t}}{(\|\mathbf{A}\| + \gamma_1 \|\mathbf{A}\|)^{k-t+1}}, \quad (12)$$

where  $k$  is the current time step and  $t = 1, 2, \dots, k$  indicates the historical time steps. Moreover,  $\gamma_1$  and  $\gamma_2$  are positive constants satisfying  $\gamma_1 \geq \gamma_2$ . It can be verified that  $\lambda_{t-1}^{(k)} \leq \lambda_t^{(k)}$  since  $\|\mathbf{A}\| > 1$  and  $\gamma_1 \geq \gamma_2$ . The reason that  $\lambda_t^{(k)}$  must be designed as in (12) is that it can ensure the convergence of the resulting estimation algorithm as shown in Section 4.

With the above preparation, we are ready to give the recursive STT algorithm that can find the optimal solution of (11). The algorithm is described as follows whereas the detailed derivation is postponed to the next subsection. In particular, consider an arbitrary initial estimate  $\hat{\mathbf{x}}_{i,0}$  and an initial process matrix estimate  $\hat{\mathbf{M}}_{i,0}$ , which is symmetric positive definite. The STT algorithm consists of three steps: *prediction*, *innovation*, and *correction*.

#### Prediction:

$$\hat{\mathbf{x}}_{i,k}^- = \mathbf{A} \hat{\mathbf{x}}_{i,k-1}, \quad (13)$$

$$\hat{\mathbf{M}}_{i,k}^- = \frac{1}{(1 + \gamma_1) \|\mathbf{A}\|} \left( \mathbf{A} \hat{\mathbf{M}}_{i,k-1} \mathbf{A}^T \right)^{-1}, \quad (14)$$

#### Innovation:

$$\mathbf{e}_{i,k}^{\text{pred}} = c \sum_{j \in (i \cup \mathcal{N}_{i,k})} \alpha_{ij,k} \mathbf{H}_{j,k}^T \mathbf{R} \left( \mathbf{z}_{j,k} - \mathbf{H}_{j,k} \hat{\mathbf{x}}_{i,k}^- \right), \quad (15)$$

$$\mathbf{e}_{i,k}^{\text{cons}} = \sum_{j \in (i \cup \mathcal{N}_{i,k})} \beta_{ij,k} \left( \hat{\mathbf{x}}_{j,k}^- - \hat{\mathbf{x}}_{i,k}^- \right), \quad (16)$$

$$\mathbf{S}_{i,k} = c \sum_{j \in (i \cup \mathcal{N}_{i,k})} \alpha_{ij,k} \mathbf{H}_{j,k}^T \mathbf{R} \mathbf{H}_{j,k} + \mathbf{I}_{6 \times 6}, \quad (17)$$

**Correction:**

$$\hat{\mathbf{M}}_{i,k} = (\gamma_2 \hat{\mathbf{M}}_{i,k}^- + \mathbf{S}_{i,k})^{-1}, \quad (18)$$

$$\hat{\mathbf{x}}_{i,k} = \hat{\mathbf{x}}_{i,k}^- + \hat{\mathbf{M}}_{i,k} (\mathbf{e}_{i,k}^{\text{pred}} + \mathbf{e}_{i,k}^{\text{cons}}). \quad (19)$$

The interpretations of the algorithm is discussed as follows.

*Prediction:* While  $\hat{\mathbf{x}}_{i,k-1}$  and  $\hat{\mathbf{M}}_{i,k-1}$  are for time  $k-1$ ,  $\hat{\mathbf{x}}_{i,k}^-$  in (13) and  $\hat{\mathbf{M}}_{i,k}^-$  in (14) are the predicted ones at time  $t$  based on the state transition model.

*Innovation:*  $\mathbf{e}_{i,k}^{\text{pred}}$  in (15) describes the prediction error and  $\mathbf{e}_{i,k}^{\text{cons}}$  in (16) denotes the consensus error. They both represent the discrepancy and hence innovation information.

*Correction:* Equation (18) corrects the value of  $\hat{\mathbf{M}}_{i,k}$  based on its prediction and the innovation information. Then,  $\hat{\mathbf{x}}_{i,k}$  is corrected in (19) based on the prediction and consensus errors.

Finally, to implement the STT algorithm, each observer must receive the following information from its neighbors:  $\{\hat{\mathbf{x}}_{j,k}^-, \mathbf{z}_{j,k}, \mathbf{H}_{j,k}\}$  where  $j \in \mathcal{N}_{i,k}$ . Here,  $\{\mathbf{z}_{j,k}, \mathbf{H}_{j,k}\}$  correspond to the measurements obtained by observer  $j$ , and  $\hat{\mathbf{x}}_{j,k}^-$  is the estimate prediction of observer  $j$ .

### 3.3 Derivation of the STT algorithm

We next present the detailed derivation of the STT algorithm proposed in the last subsection.

1) First, we derive the closed-form solution that can minimize the objective function in (11). In particular, the gradient of  $J(\hat{\mathbf{x}}_{i,k})$  is

$$\nabla_{\hat{\mathbf{x}}_{i,k}} J(\hat{\mathbf{x}}_{i,k}) = 2 \left( \sum_{t=1}^k \lambda_t^{(k)} \mathbf{S}_{i,t}^{(k)} \right) \hat{\mathbf{x}}_{i,k} - 2 \left( \sum_{t=1}^k \lambda_t^{(k)} \mathbf{y}_{i,t}^{(k)} \right),$$

where

$$\mathbf{y}_{i,t}^{(k)} = (\mathbf{A}^{t-k})^T \left[ \sum_{j \in (i \cup \mathcal{N}_{i,t})} (c\alpha_{ij,t} \mathbf{H}_{j,t}^T \mathbf{R} \mathbf{z}_{j,t} + \beta_{ij,t} \hat{\mathbf{x}}_{j,t}^-) \right], \quad (20)$$

$$\mathbf{S}_{i,t}^{(k)} = (\mathbf{A}^{t-k})^T \left[ \sum_{j \in (i, \mathcal{N}_{i,t})} (c\alpha_{ij,t} \mathbf{H}_{j,t}^T \mathbf{R} \mathbf{H}_{j,t}) + \mathbf{I}_6 \right] \mathbf{A}^{t-k}. \quad (21)$$

Note that  $\mathbf{y}_{i,t}^{(k)}$  and  $\mathbf{S}_{i,t}^{(k)}$  depend on both  $t$  and  $k$ . When  $t = k$ , we have  $\mathbf{S}_{i,k}^{(k)} \doteq \mathbf{S}_{i,k}$ . By solving  $\nabla_{\hat{\mathbf{x}}_{i,k}} J(\hat{\mathbf{x}}_{i,k}) = 0$ ,

we can obtain the closed-form solution as

$$\hat{\mathbf{x}}_{i,k} = \left( \sum_{t=1}^k \lambda_t^{(k)} \mathbf{S}_{i,t}^{(k)} \right)^{-1} \left( \sum_{t=1}^k \lambda_t^{(k)} \mathbf{y}_{i,t}^{(k)} \right). \quad (22)$$

It should be noted that (22) cannot be implemented in practice because it involves all the historical information before time step  $k$ . We need to derive a recursive expression.

2) Second, we derive the recursive expression of the optimal solution in (22). To do that, define

$$\begin{aligned} \hat{\mathbf{M}}_{i,k} &\doteq \lambda_k^{(k)} \left( \sum_{t=1}^k \lambda_t^{(k)} \mathbf{S}_{i,t}^{(k)} \right)^{-1}, \\ \bar{\mathbf{y}}_{i,k} &\doteq \frac{1}{\lambda_k^{(k)}} \sum_{t=1}^k \lambda_t^{(k)} \mathbf{y}_{i,t}^{(k)}. \end{aligned} \quad (23)$$

Then,  $\hat{\mathbf{x}}_{i,k}$  in (22) can be rewritten as

$$\hat{\mathbf{x}}_{i,k} = \hat{\mathbf{M}}_{i,k} \bar{\mathbf{y}}_{i,k}. \quad (24)$$

We next derive the recursive forms of  $\hat{\mathbf{M}}_{i,k}$  and  $\bar{\mathbf{y}}_{i,k}$ , respectively, to obtain the recursive form of  $\hat{\mathbf{x}}_{i,k}$ . First of all, the relationship between  $\mathbf{S}_{i,t}^{(k-1)}$  and  $\mathbf{S}_{i,t}^{(k)}$ ,  $\lambda_t^{(k-1)}$  and  $\lambda_t^{(k)}$  can be obtained from (21) and (12) as

$$\begin{aligned} \mathbf{S}_{i,t}^{(k-1)} &= \mathbf{A}^T \mathbf{S}_{i,t}^{(k)} \mathbf{A}, \\ \lambda_t^{(k-1)} &= \frac{\|\mathbf{A}\|(1 + \gamma_1)}{\gamma_2} \lambda_t^{(k)} = \frac{1}{\lambda_k^{(k)} \gamma_2} \lambda_t^{(k)}. \end{aligned}$$

Similarly, the relationship between  $\mathbf{y}_t^{(k-1)}$  and  $\mathbf{y}_t^{(k)}$  can be obtained from (20):

$$\mathbf{y}_t^{(k-1)} = \mathbf{A}^T \mathbf{y}_t^{(k)}.$$

Then,  $\hat{\mathbf{M}}_{i,k-1}$  can be rewritten as

$$\begin{aligned} \hat{\mathbf{M}}_{i,k-1} &= \lambda_{k-1}^{(k-1)} \left( \sum_{t=1}^{k-1} \lambda_t^{(k-1)} \mathbf{S}_{i,t}^{(k-1)} \right)^{-1} \\ &= \gamma_2 \left( \lambda_{k-1}^{(k-1)} \right)^2 \left( \sum_{t=1}^{k-1} \lambda_t^{(k)} \mathbf{A}^T \mathbf{S}_{i,t}^{(k)} \mathbf{A} \right)^{-1} \\ &= \gamma_2 \left( \lambda_{k-1}^{(k-1)} \right)^2 \mathbf{A}^{-1} \left( \sum_{t=1}^{k-1} \lambda_t^{(k)} \mathbf{S}_{i,t}^{(k)} \right)^{-1} (\mathbf{A}^T)^{-1}. \end{aligned}$$

Taking matrix inverse on both sides of the above equa-

tion gives

$$\begin{aligned}\sum_{t=1}^{k-1} \lambda_t^{(k)} \mathbf{S}_{i,t}^{(k)} &= \gamma_2 \left( \lambda_{k-1}^{(k-1)} \right)^2 (\mathbf{A} \hat{\mathbf{M}}_{i,k-1} \mathbf{A}^T)^{-1} \\ &= \gamma_2 \left( \lambda_k^{(k)} \right)^2 (\mathbf{A} \hat{\mathbf{M}}_{i,k-1} \mathbf{A}^T)^{-1}.\end{aligned}$$

Since  $\lambda_{k-1}^{(k-1)} = 1/(\|\mathbf{A}\|(1 + \gamma_1)) = \lambda_k^{(k)}$  by definition, substituting the above equation into (23) yields

$$\begin{aligned}\hat{\mathbf{M}}_{i,k} &= \lambda_k^{(k)} \left( \sum_{t=1}^k \lambda_t^{(k)} \mathbf{S}_{i,t}^{(k)} \right)^{-1} \\ &= \left[ \frac{1}{\lambda_k^{(k)}} \left( \sum_{t=1}^{k-1} \lambda_t^{(k)} \mathbf{S}_{i,t}^{(k)} \right) + \mathbf{S}_{i,k}^{(k)} \right]^{-1} \\ &= \left[ \gamma_2 \lambda_k^{(k)} (\mathbf{A} \hat{\mathbf{M}}_{i,k-1} \mathbf{A}^T)^{-1} + \mathbf{S}_{i,k}^{(k)} \right]^{-1} \\ &= \left( \gamma_2 \hat{\mathbf{M}}_{i,k}^- + \mathbf{S}_{i,k}^{(k)} \right)^{-1},\end{aligned}$$

where  $\hat{\mathbf{M}}_{i,k}^-$  is given in (14).

Similarly, the recursive form of  $\bar{\mathbf{y}}_{i,k}$  can be derived as

$$\begin{aligned}\bar{\mathbf{y}}_{i,k} &= \frac{1}{\lambda_k^{(k)}} \sum_{t=1}^k \lambda_t^{(k)} \mathbf{y}_{i,t}^{(k)} \\ &= \left( \frac{1}{\|\mathbf{A}\|(1 + \gamma_1)} \sum_{t=1}^{k-1} \lambda_t^{(k)} \mathbf{y}_{i,t}^{(k)} + \mathbf{y}_{i,k}^{(k)} \right) \\ &= \gamma_2 (\mathbf{A}^T)^{-1} \sum_{t=1}^{k-1} \lambda_t^{(k-1)} \mathbf{y}_{i,t}^{(k-1)} + \mathbf{y}_{i,k}^{(k)} \\ &= \frac{\gamma_2}{\|\mathbf{A}\| + \gamma_1 \|\mathbf{A}\|} (\mathbf{A}^T)^{-1} \bar{\mathbf{y}}_{i,k-1} + \mathbf{y}_{i,k}^{(k)}.\end{aligned}\quad (25)$$

3) Third, since  $\mathbf{S}_{i,k}^{(k)}$  and  $\hat{\mathbf{M}}_{i,k}^-$  are symmetric positive definition matrices, we have

$$\hat{\mathbf{M}}_{i,k} = \left[ \mathbf{I}_6 - \left( \gamma_2 (\mathbf{S}_{i,k}^{(k)})^{-1} \hat{\mathbf{M}}_{i,k}^- + \mathbf{I}_6 \right)^{-1} \right] \frac{1}{\gamma_2} \left( \hat{\mathbf{M}}_{i,k}^- \right)^{-1}, \quad (26)$$

based on the preliminary fact in (9). Substituting (25) and (26) into (24) yields the recursive form of  $\hat{\mathbf{x}}_{i,k}$ :

$$\begin{aligned}\hat{\mathbf{x}}_{i,k} &= \mathbf{A} \hat{\mathbf{x}}_{i,k-1} - \hat{\mathbf{M}}_{i,k} \mathbf{S}_{i,k}^{(k)} \hat{\mathbf{x}}_{i,k-1} + \hat{\mathbf{M}}_{i,k} \mathbf{y}_{i,k}^{(k)} \\ &= \hat{\mathbf{x}}_{i,k}^- + \hat{\mathbf{M}}_{i,k} \left( \mathbf{y}_{i,k}^{(k)} - \mathbf{S}_{i,k}^{(k)} \hat{\mathbf{x}}_{i,k}^- \right),\end{aligned}$$

where  $\hat{\mathbf{x}}_{i,k}^-$  is given in (13) and  $\mathbf{y}_{i,k}^{(k)} - \mathbf{S}_{i,k}^{(k)} \hat{\mathbf{x}}_{i,k}^-$  can be

split into

$$\begin{aligned}\mathbf{y}_{i,k}^{(k)} - \mathbf{S}_{i,k}^{(k)} \hat{\mathbf{x}}_{i,k}^- &= \sum_{j \in (i \cup \mathcal{N}_{i,k})} (c \alpha_{ij,t} \mathbf{H}_{j,k}^T \mathbf{R} \mathbf{z}_{j,k} + \beta_{ij,k} \hat{\mathbf{x}}_{j,k}^-) \\ &\quad - \sum_{j \in (i, \mathcal{N}_{i,k})} (c \alpha_{ij,k} \mathbf{H}_{j,k}^T \mathbf{R} \mathbf{H}_{j,k}) \hat{\mathbf{x}}_{i,k}^- - \hat{\mathbf{x}}_{i,k}^- \\ &= c \sum_{j \in (i \cup \mathcal{N}_{i,k})} \alpha_{ij,k} \mathbf{H}_{j,k}^T \mathbf{R} (\mathbf{z}_{j,k} - \mathbf{H}_{j,k} \hat{\mathbf{x}}_{i,k}^-) \\ &\quad + \sum_{j \in (i \cup \mathcal{N}_{i,k})} \beta_{ij,k} (\hat{\mathbf{x}}_{j,k}^- - \hat{\mathbf{x}}_{i,k}^-) \\ &= \mathbf{e}_{i,k}^{\text{pred}} + \mathbf{e}_{i,k}^{\text{cons}},\end{aligned}$$

where  $\mathbf{e}_{i,k}^{\text{pred}}$  and  $\mathbf{e}_{i,k}^{\text{cons}}$  are given in (15) and (16), respectively.

#### 4 Convergence Analysis

The STT algorithm in (13)-(19) is executed by a single observer. Since each observer's estimation relies on other observers' estimation, we need to prove that the overall interconnected system is convergent. The aim of the convergence analysis is to show that the expectation of the error converges to zero.

Suppose the current time step is  $k$ . The estimation error of observer  $i$  is denoted as  $\boldsymbol{\eta}_{i,k} \doteq \hat{\mathbf{x}}_{i,k} - \mathbf{x}_k$ . It follows from (22) that

$$\begin{aligned}\boldsymbol{\eta}_{i,k} &= \hat{\mathbf{x}}_{i,k} - \mathbf{x}_k \\ &= \left( \sum_{t=1}^k \lambda_t^{(k)} \mathbf{S}_{i,t}^{(k)} \right)^{-1} \sum_{t=1}^k \lambda_t^{(k)} \mathbf{y}_{i,t}^{(k)} \\ &\quad - \left( \sum_{t=1}^k \lambda_t^{(k)} \mathbf{S}_{i,t}^{(k)} \right)^{-1} \left( \sum_{t=1}^k \lambda_t^{(k)} \mathbf{S}_{i,t}^{(k)} \right) \mathbf{x}_k \\ &= \left( \sum_{t=1}^k \lambda_t^{(k)} \mathbf{S}_{i,t}^{(k)} \right)^{-1} \left[ \sum_{t=1}^k \lambda_t^{(k)} (\mathbf{y}_{i,t}^{(k)} - \mathbf{S}_{i,t}^{(k)} \mathbf{x}_k) \right],\end{aligned}$$

where  $\mathbf{y}_{i,t}^{(k)}$  and  $\mathbf{S}_{i,t}^{(k)}$  are given in (20) and (21), respectively.

We next derive the expression of the expectation of  $\boldsymbol{\eta}_{i,k}$ .

**Lemma 1 (Expression of  $\mathbb{E}[\boldsymbol{\eta}_{i,k}]$ )** *The expectation of  $\boldsymbol{\eta}_{i,k}$  is expressed as*

$$\mathbb{E}[\boldsymbol{\eta}_{i,k}] = \left( \sum_{t=1}^k \lambda_t^{(k)} \mathbf{S}_{i,t}^{(k)} \right)^{-1} \mathbb{E}[\bar{\boldsymbol{\eta}}_{i,k}], \quad (27)$$

where

$$\bar{\boldsymbol{\eta}}_{i,k} \doteq \sum_{t=1}^k \left[ \lambda_t^{(k)} (\mathbf{A}^{t-k})^T \sum_{j \in (i \cup \mathcal{N}_{i,t})} (\beta_{ij,t} \mathbf{A} \boldsymbol{\eta}_{j,t-1}) \right]. \quad (28)$$

**Proof 1** See Appendix 7.1.

To prove that  $\mathbb{E}[\boldsymbol{\eta}_{i,k}]$  converges to zero, we analyze its upper bound. It follows from (27) that

$$\begin{aligned} \|\mathbb{E}[\boldsymbol{\eta}_{i,k}]\| &\leq \left\| \left( \sum_{t=1}^k \lambda_t^{(k)} \mathbf{S}_{i,t}^{(k)} \right)^{-1} \right\| \|\mathbb{E}[\bar{\boldsymbol{\eta}}_{i,k}]\| \\ &= \frac{1}{\sigma_{\min} \left( \sum_{t=1}^k \lambda_t^{(k)} \mathbf{S}_{i,t}^{(k)} \right)} \|\mathbb{E}[\bar{\boldsymbol{\eta}}_{i,k}]\|. \end{aligned} \quad (29)$$

In the following, we establish Lemma 2 to Lemma 6 to prove that

$$\sigma_{\min} \left( \sum_{t=1}^k \lambda_t^{(k)} \mathbf{S}_{i,t}^{(k)} \right) \geq 1. \quad (30)$$

This fact is nontrivial to prove and it is a unique challenge for analyze bearing-only cooperative estimation. Although  $\mathbf{S}_{i,t}^{(k)}$  is positive definite as shown in (21), given the expression of  $\lambda_t^{(k)}$  in (12), we are not able to trivially claim that (30) is valid because  $\mathbf{H}_{j,t}^T \mathbf{R} \mathbf{H}_{j,t}$  in (21) is rank deficient. We must carefully explore the intrinsic structure of  $\mathbf{H}_{j,t}$  and analyze the properties of orthogonal projection matrices embedded in there.

**Lemma 2 (Expression of  $\sum_{t=1}^k \lambda_t^{(k)} \mathbf{S}_{i,t}^{(k)}$ )** The expression of  $\sum_{t=1}^k \lambda_t^{(k)} \mathbf{S}_{i,t}^{(k)}$  is given by

$$\begin{aligned} &\sum_{t=1}^k \lambda_t^{(k)} \mathbf{S}_{i,t}^{(k)} \\ &= \frac{c}{\sigma_v^2} \sum_{t=1}^k \lambda_t^{(k)} \mathbf{F}_t^{(k)} \otimes \bar{\mathbf{P}}_{i,t} + \sum_{t=1}^k \lambda_t^{(k)} (\mathbf{A}^{t-k})^T \mathbf{A}^{t-k}, \end{aligned} \quad (31)$$

where

$$\mathbf{F}_t^{(k)} \doteq \begin{bmatrix} 1 & (t-k)\Delta t \\ (t-k)\Delta t & (t-k)^2 \Delta t^2 \end{bmatrix}, \quad (32)$$

and

$$\bar{\mathbf{P}}_{i,t} \doteq \sum_{j \in (i \cup \mathcal{N}_{i,t})} \alpha_{ij,t} \mathbf{P}_{j,t}. \quad (33)$$

Here,  $\mathbf{P}_{i,t}$  is a concise notation of  $\mathbf{P}_{\tilde{\mathbf{g}}_{i,t}}$ , where  $\tilde{\mathbf{g}}_{i,t}$  is the bearing vector measured by observer  $i$  at time step  $t$ . The matrix operator  $\mathbf{P}$  is defined in (5).

**Proof 2** See Appendix 7.2.

Lemma 2 indicates that, to analyze  $\sigma_{\min} \left( \sum_{t=1}^k \lambda_t^{(k)} \mathbf{S}_{i,t}^{(k)} \right)$ , we need first analyze  $\sigma_{\min}(\bar{\mathbf{P}}_{i,t})$  and  $\sigma_{\min} \left( \sum_{t=1}^k \lambda_t^{(k)} \mathbf{F}_t^{(k)} \right)$ .

On the one hand, we analyze the lower bound of  $\sigma_{\min}(\bar{\mathbf{P}}_{i,t})$ . The next is a useful result for the orthogonal projection matrices defined in 33.

**Lemma 3 (Value of  $\sigma_{\min}(\mathbf{P}_{i,t} + \mathbf{P}_{j,t})$ )** Suppose that  $\mathbf{g}_{i,t}$  and  $\mathbf{g}_{j,t}$  are two bearing vectors and  $\theta_{ij,t} \in [0, \pi)$  is the angle between the two vectors. If  $\mathbf{P}_{i,t} = \mathbf{I}_{3 \times 3} - \mathbf{g}_{i,t} \mathbf{g}_{i,t}^T$  and  $\mathbf{P}_{j,t} = \mathbf{I}_{3 \times 3} - \mathbf{g}_{j,t} \mathbf{g}_{j,t}^T$ , then

$$\sigma_{\min}(\mathbf{P}_{i,t} + \mathbf{P}_{j,t}) = 1 - |\cos \theta_{ij,t}|.$$

**Proof 3** See Appendix 7.3.

Lemma 3 reveals the unique property of the orthogonal projection matrices. It indicates that, when the two bearings are not parallel, the matrix  $\mathbf{P}_{i,t} + \mathbf{P}_{j,t}$  is nonsingular. Intuitively, this property corresponds to the triangulation geometry that observers must observe from different directions. It is essential to prove the convergence of the algorithm.

With Lemma 3, we can analyze the lower bound of  $\sigma_{\min}(\bar{\mathbf{P}}_{i,t})$ .

**Lemma 4 (Lower bound of  $\sigma_{\min}(\bar{\mathbf{P}}_{i,t})$ )** For observer  $i$ , suppose there exists  $\alpha_0 > 0$  such that

$$\alpha_{ij,t} \geq \alpha_0, \quad \text{for all } j \in \mathcal{N}_{i,t}. \quad (34)$$

If there exists  $j \in (i \cup \mathcal{N}_{i,t})$  such that the angle  $\theta_{ij,t}$  between  $\tilde{\mathbf{g}}_{i,t}$  and  $\tilde{\mathbf{g}}_{j,t}$  satisfies

$$0 < \theta_0 \leq \theta_{ij,t} \leq \pi - \theta_0 < \pi, \quad (35)$$

where  $\theta_0 \in (0, \pi/2)$ , then we have

$$\sigma_{\min}(\bar{\mathbf{P}}_{i,t}) \geq \alpha_0(1 - \cos \theta_0).$$

**Proof 4** It follows from the definition of  $\bar{\mathbf{P}}_{i,t}$  that

$$\begin{aligned} &\sigma_{\min}(\bar{\mathbf{P}}_{i,t}) \\ &\geq \alpha_0 \sigma_{\min} \left( \sum_{j \in (i \cup \mathcal{N}_{i,t})} \mathbf{P}_{j,t} \right) \quad (\text{due to } \alpha_{ij,t} \geq \alpha_0) \\ &\geq \alpha_0 \sigma_{\min}(\mathbf{P}_{i,t} + \mathbf{P}_{j,t}) \quad (\text{only consider } i, j) \\ &= \alpha_0(1 - |\cos \theta_{ij,t}|) \quad (\text{by Lemma 3}) \\ &\geq \alpha_0(1 - \cos \theta_0), \end{aligned}$$



where last inequality is because  $|\cos \theta_{ij,t}| \geq \cos \theta_0$  due to (35).

The assumption in (34) is reasonable. In particular, since  $\sum_{j \in \mathcal{N}_i} \alpha_{ij,t} = 1$ , we can choose

$$\alpha_{ij,t} = \frac{1}{1 + |\mathcal{N}_{i,t}|}, \quad j \in \mathcal{N}_i.$$

As a result, (34) is equivalent to the assumption that  $|\mathcal{N}_{i,t}|$  is finite, which is true in practice.

On the other hand, we analyze  $\sigma_{\min}(\sum_{t=1}^k \lambda_t^{(k)} \mathbf{F}_t^{(k)})$ .

**Lemma 5 (Lower bound of  $\sigma_{\min}(\sum_{t=1}^k \lambda_t^{(k)} \mathbf{F}_t^{(k)})$ )**  
It holds that

$$\sigma_{\min} \left( \sum_{t=1}^k \lambda_t^{(k)} \mathbf{F}_t^{(k)} \right) \geq \lambda_{k-1}^{(k)} f(\Delta t),$$

where  $f(\Delta t) = (2 + \Delta t^2 - \sqrt{4 + \Delta t^4}) / 2$ .

**Proof 5** See Appendix 7.4.

With Lemma 4 and Lemma 5, we are ready to analyze  $\sigma_{\min}(\sum_{t=1}^k \lambda_t^{(k)} \mathbf{S}_{i,t}^{(k)})$ .

**Lemma 6 (Lower bound of  $\sigma_{\min}(\sum_{t=1}^k \lambda_t^{(k)} \mathbf{S}_{i,t}^{(k)})$ )**

Given  $\lambda_t^{(k)}$  defined in (12), if  $c$  satisfies

$$\begin{aligned} c &\geq \frac{(1 - \lambda_k^{(k)}) \sigma_{\mathbf{v}}^2}{\lambda_{k-1}^{(k)} f(\Delta t) \alpha_0 (1 - \cos \theta_0)} \\ &= \frac{(\|\mathbf{A}\| (1 + \gamma_1) - 1) \|\mathbf{A}\| (1 + \gamma_1) \sigma_{\mathbf{v}}^2}{\gamma_2 f(\Delta t) \alpha_0 (1 - \cos \theta_0)}, \end{aligned} \quad (36)$$

then it holds that

$$\sigma_{\min} \left( \sum_{t=1}^k \lambda_t^{(k)} \mathbf{S}_{i,t}^{(k)} \right) \geq 1.$$

**Proof 6** See Appendix 7.5.

Finally, we can prove main result that  $\|\mathbb{E}[\boldsymbol{\eta}_{i,t}]\|$  converges.

**Theorem 1 (Convergence of  $\|\mathbb{E}[\boldsymbol{\eta}_{i,t}]\|$ )** Given  $\lambda_t^{(k)}$  defined in (12), if (34) and (35) holds and  $\gamma_1 > \gamma_2$ , then  $\|\mathbb{E}[\boldsymbol{\eta}_{i,k}]\|$  converges to zero exponentially fast for all  $i \in \mathcal{V}$  as  $k \rightarrow \infty$ .

**Proof 7** Since  $\sigma_{\min}(\sum_{t=1}^k \lambda_t^{(k)} \mathbf{S}_{i,t}^{(k)}) \geq 1$  according to Lemma 6, it follows from (29) that

$$\|\mathbb{E}[\boldsymbol{\eta}_{i,k}]\| \leq \|\mathbb{E}[\bar{\boldsymbol{\eta}}_{i,k}]\| \leq \max_{j \in \mathcal{V}} \|\mathbb{E}[\bar{\boldsymbol{\eta}}_{j,k}]\|, \quad (37)$$

where  $\mathcal{V} = \{1, \dots, n\}$ . With the definition of  $\bar{\boldsymbol{\eta}}_{i,k}$  in (28), we have

$$\begin{aligned} \mathbb{E}[\bar{\boldsymbol{\eta}}_{i,k}] &= \lambda_k^{(k)} \sum_{j \in (i \cup \mathcal{N}_{i,k})} \beta_{ij,k-1} \mathbf{A} \mathbb{E}[\boldsymbol{\eta}_{j,k-1}] \\ &\quad + \sum_{t=1}^{k-1} \lambda_t^{(k)} (\mathbf{A}^T)^{t-k} \sum_{j \in (i \cup \mathcal{N}_{i,t})} \beta_{ij,t-1} \mathbf{A} \mathbb{E}[\boldsymbol{\eta}_{j,t-1}] \\ &= \lambda_k^{(k)} \sum_{j \in (i \cup \mathcal{N}_{i,k})} \beta_{ij,k-1} \mathbf{A} \mathbb{E}[\boldsymbol{\eta}_{j,k-1}] \\ &\quad + \frac{\gamma_2}{\|\mathbf{A}\| (1 + \gamma_1)} (\mathbf{A}^T)^{-1} \\ &\quad \cdot \underbrace{\sum_{t=1}^{k-1} \lambda_t^{(k-1)} (\mathbf{A}^T)^{t-(k-1)} \sum_{j \in (i \cup \mathcal{N}_{i,t})} \beta_{ij,t-1} \mathbf{A} \mathbb{E}[\boldsymbol{\eta}_{j,t-1}]}_{\mathbb{E}[\bar{\boldsymbol{\eta}}_{i,k-1}]} \\ &= \frac{1}{(1 + \gamma_1) \|\mathbf{A}\|} \sum_{j \in (i \cup \mathcal{N}_{i,k})} \beta_{ij,k-1} \mathbf{A} \mathbb{E}[\boldsymbol{\eta}_{j,k-1}] \\ &\quad + \frac{\gamma_2}{(1 + \gamma_1) \|\mathbf{A}\|} (\mathbf{A}^T)^{-1} \mathbb{E}[\bar{\boldsymbol{\eta}}_{i,k-1}]. \end{aligned}$$

Taking norm on both sides of the above equation gives

$$\begin{aligned} \|\mathbb{E}[\bar{\boldsymbol{\eta}}_{i,k}]\| &\leq \frac{1}{(1 + \gamma_1) \|\mathbf{A}\|} \sum_{j \in (i \cup \mathcal{N}_{i,k})} \beta_{ij,k} \|\mathbf{A}\| \|\mathbb{E}[\boldsymbol{\eta}_{j,k-1}]\| \\ &\quad + \frac{\gamma_2}{(1 + \gamma_1) \|\mathbf{A}\|} \|(\mathbf{A}^T)^{-1}\| \|\mathbb{E}[\bar{\boldsymbol{\eta}}_{i,k-1}]\|. \end{aligned}$$

Since  $\sum_{j \in (i, \mathcal{N}_{i,k})} \beta_{ij,k} = 1$  and  $\|\mathbb{E}[\bar{\boldsymbol{\eta}}_{i,k-1}]\| \leq \max_{j \in \mathcal{V}} \|\mathbb{E}[\bar{\boldsymbol{\eta}}_{j,k-1}]\|$ , substituting (37) into the above inequality yields

$$\begin{aligned} \|\mathbb{E}[\bar{\boldsymbol{\eta}}_{i,k}]\| &\leq \frac{1}{(1 + \gamma_1) \|\mathbf{A}\|} \sum_{j \in (i \cup \mathcal{N}_{i,k})} \beta_{ij,k} \|\mathbf{A}\| \max_{j \in \mathcal{V}} \|\mathbb{E}[\bar{\boldsymbol{\eta}}_{j,k-1}]\| \\ &\quad + \frac{\gamma_2}{(1 + \gamma_1) \|\mathbf{A}\|} \|(\mathbf{A}^T)^{-1}\| \max_{j \in \mathcal{V}} \|\mathbb{E}[\bar{\boldsymbol{\eta}}_{j,k-1}]\| \\ &= \frac{1}{(1 + \gamma_1)} \max_{j \in \mathcal{V}} \|\mathbb{E}[\bar{\boldsymbol{\eta}}_{j,k-1}]\| \\ &\quad + \frac{\gamma_2}{(1 + \gamma_1) \|\mathbf{A}\|} \|(\mathbf{A}^T)^{-1}\| \max_{j \in \mathcal{V}} \|\mathbb{E}[\bar{\boldsymbol{\eta}}_{j,k-1}]\|. \end{aligned}$$

It can be verified that the matrix  $\mathbf{A}$  defined in (4) satisfies  $\|(\mathbf{A}^T)^{-1}\| = \|\mathbf{A}\|$ . Then, we have

$$\begin{aligned} \|\mathbb{E}[\bar{\boldsymbol{\eta}}_{i,k}]\| &\leq \frac{1}{(1 + \gamma_1)} \max_{j \in \mathcal{V}} \|\mathbb{E}[\bar{\boldsymbol{\eta}}_{j,k-1}]\| \\ &\quad + \frac{\gamma_2}{(1 + \gamma_1)} \max_{j \in \mathcal{V}} \|\mathbb{E}[\bar{\boldsymbol{\eta}}_{j,k-1}]\| \\ &\leq \frac{1 + \gamma_2}{1 + \gamma_1} \max_{j \in \mathcal{V}} \|\mathbb{E}[\bar{\boldsymbol{\eta}}_{j,k-1}]\|. \end{aligned}$$

Since the above inequality holds for any  $i \in \mathcal{V}$ , we have

$$\max_{i \in \mathcal{V}} \|\mathbb{E}[\tilde{\mathbf{n}}_{i,k}]\| \leq \frac{1 + \gamma_2}{1 + \gamma_1} \max_{j \in \mathcal{V}} \|\mathbb{E}[\tilde{\mathbf{n}}_{j,k-1}]\|.$$

and hence

$$\max_{i \in \mathcal{V}} \|\mathbb{E}[\tilde{\mathbf{n}}_{i,k}]\| \leq \left( \frac{1 + \gamma_2}{1 + \gamma_1} \right)^{k-1} \max_{j \in \mathcal{V}} \|\mathbb{E}[\tilde{\mathbf{n}}_{j,1}]\|. \quad (38)$$

If  $\gamma_1 > \gamma_2$ , then  $(1 + \gamma_2)/(1 + \gamma_1) < 1$  and hence  $\max_{i \in \mathcal{V}} \|\mathbb{E}[\tilde{\mathbf{n}}_{i,k}]\| \rightarrow 0$  as  $k \rightarrow \infty$ . Since  $\|\mathbb{E}[\tilde{\mathbf{n}}_{i,k}]\| \leq \max_{i \in \mathcal{V}} \|\mathbb{E}[\tilde{\mathbf{n}}_{i,k}]\|$  for all  $i \in \mathcal{V}$ , we know that  $\|\mathbb{E}[\tilde{\mathbf{n}}_{i,k}]\|$  also converges to zero exponentially fast.

Regarding the convergence rate, it can be seen from (38) that the convergence rate is determined by  $\gamma_1, \gamma_2$ , which are the two parameters in the forgetting factor defined in (12). When  $\gamma_2$  is much less than  $\gamma_1$  and hence the forgetting factor is small, then the convergence rate is also small and hence the convergence is fast.

## 5 Numerical Simulation

In this section, the performance of the proposed STT algorithm is evaluated and compared with the DKF algorithms including consensus on measurement Kalman filter (CMKF) [15], consensus on information Kalman filter (CIKF), and hybrid consensus on information and consensus on measurement Kalman filter (HCMCI-KF) [17]. The details of these algorithms are given in Appendix 7.6. A benchmark algorithm, the centralized Kalman filter (CKF), is also used as a baseline for comparison. We will see that the proposed STT algorithm achieves better performance than the algorithms and comparable performance as the CKF.

### 5.1 Simulation setup

Consider a 3D cube with the side lengths as  $80 \times 80 \times 40$ . In every simulation trial, a set of  $n = 10$  observers are randomly placed inside the 3D cube. The initial estimate of every observer is selected as  $\hat{\mathbf{x}}_{i,0} = \mathbf{s}_{i,0}$ . It is supposed that each observer can always measure the moving target's bearing and each observer can only obtain the information from its three nearest neighbors. The locations of the observers and the network topology are invariant in each simulation trial. They are however different across different simulation trials.

To ensure a fair comparison between the STT algorithm and the other DKF algorithms, we used the genetic algorithm (GA) toolbox in Matlab to optimize the parameters. For the STT algorithm, the optimized parameter values are  $c = 1.8202$ ,  $\gamma_1 = 7.1609$ , and  $\gamma_2 = 6.1323$ . Moreover,  $\alpha_{ij,k} = \beta_{ij,k} = 1/(1 + |\mathcal{N}_{i,k}|) = 0.25$  since

Table 1  
Parameters of the DKF algorithms

Parameters	$a_0$	$a_1$	$a_2$	$\beta$
CKF	2.5410	0.0033	0.0070	0.1
CMKF	26.5483	0.1325	0.2390	0.25
CIKF	23.1375	0.8987	0.2988	1/3
HCMCI-KF	3.9219	0.0542	0.0804	0.25

each observer has three neighbors (i.e.,  $|\mathcal{N}_{i,k}| = 3$ ). The DKF algorithms rely on two parameters  $\mathbf{R}$  and  $\mathbf{Q}$ :

$$\mathbf{R} = a_0 \mathbf{I}_3, \\ \mathbf{Q} = \begin{bmatrix} a_1 \mathbf{I}_{3 \times 3} & \mathbf{0}_{3 \times 3} \\ \mathbf{I}_{3 \times 3} & a_2 \mathbf{I}_{3 \times 3} \end{bmatrix},$$

where  $a_0, a_1$ , and  $a_2$  are positive constant coefficients. Their values are optimized by GA and given in Table 1. The value  $\beta$  is a positive constant coefficient correlated to the number of neighboring nodes as given in Appendix 7.6. Moreover, the HCMCI-KF algorithm has other two parameters  $L$  and  $\omega$ . In particular, HCMCI-KF has an iterative process embedded inside each iteration step. The parameter  $L$  is the number of iterations of the embedded iterative process. Here, it is set as  $L = 1$ .  $\omega$  is a weight of the neighbors' information and is set to  $\omega = 4$ . Finally, the sampling interval  $\Delta t$  is set to 0.1.

### 5.2 Evaluation results: Accuracy and convergence rate

Here, we consider two simulation scenarios. In the first scenario, we suppose the target moves along a circle. This scenario is important to study because the target's motion has a nonzero time-varying acceleration and is different from the assumed dynamic model in (4). The initial position of the target is  $\mathbf{p}_0 = [15, 0, 5]^T$ , and its velocity is  $\mathbf{v}(t) = 5[\sin(t/10\pi), \cos(t/10\pi), 0]^T$ . In the second scenario, we suppose the target moves along a square. This scenario is important to study because the target has abrupt motion at the corners, which are important to evaluate the algorithms' convergence rate. In this scenario, the target's initial position is  $\mathbf{p}_0 = [20, 20, 5]^T$ , and the initial velocity is  $\mathbf{v}(0) = [0, -4, 0]^T$ . The velocity direction rotates clockwise by  $90^\circ$  every six seconds.

A zero-mean Gaussian noise is added to each bearing measurement based on (2) in the simulations. The standard deviation is  $0.1 \text{ rad} \approx 5.73^\circ$ . In the following, each simulation result is an average over 100 simulation trials. An example of the network topology and the estimation trajectories are shown in Fig. 1. The estimation errors in terms of average root-mean-square-error (RMSE) are shown in Fig. 2 and Fig. 3.

Compared to the DKF algorithms, the STT algorithms achieves the *smallest* position and velocity estimation

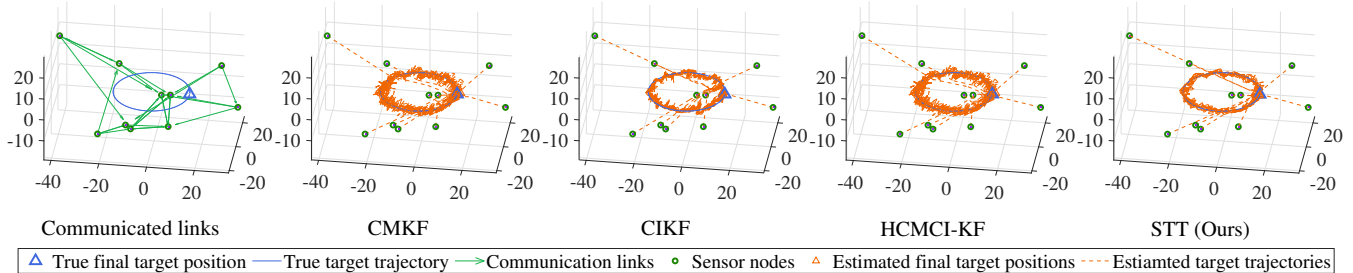


Fig. 1. Circle shape motion target state estimation with fixed 10 observers. Each observer can obtain the closest 3 neighboring nodes' information. The performances of CMKF, CIKF, HCMCI-KF, and STT (Ours) algorithms in that order.

errors. The accuracy of velocity estimation is comparable to the CKF. STT also achieves the *fastest* convergence rate. This is important because it indicates that STT has a better ability to track highly maneuverable targets. The performance of STT is comparable to the CKF due to the carefully-designed objective function and the optimality of the DRLS framework. In addition, among the DKF algorithms, HCICM-KF achieves better performance than CIKF and CMKF.

### 5.3 Evaluation results: Impact of noise

We now evaluate the impact of the measurement noises on the estimation accuracy. We consider the case where the target moves along a square. Here, the standard deviation of the zero-mean Gaussian noise added to each bearing measurement varies from 0.01 rad to 0.3 rad. Each simulation result is an average of 100 times simulation trials.

The simulation results are shown in Fig. 4. It can be seen that the accuracy for both position and velocity estimation drops as the noise's standard deviation increases. However, STT has the best accuracy across different noise levels compared to the other algorithms.

## 6 Experimental Verification

We implemented the proposed STT algorithm in a real-world vision-based cooperative aerial target pursuit system to verify its effectiveness under practical conditions.

The system consists of three pursuer MAVs (DJI M300) and one target MAV (DJI Phantom 4). See Fig. 5a for illustration. Each pursuer MAV uses its onboard camera to detection, localize, and follow the target MAV. The key specifications of each pursuer MAV is shown in Table 2.

The overall system is fully autonomously and all the functions are realized onboard. The detection, estimation, and control components form a closed loop, where the former one's output is the later one's input. To

Table 2

Key specifications of the pursuer MAV

Parameter	Value	Unit
Dimension	810x670	mm
Mass	6.3	kg
Max takeoff weight	9	kg
FOV of the gimbal camera	82.9	degree
Video Resolution	1920x1080	pix
Frame rate	30	FPS
Communicate rate	10	Hz

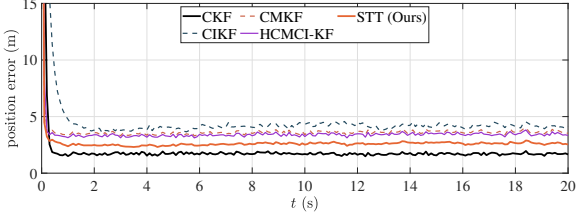
the best of our knowledge, it is also the first fully autonomous vision-based cooperative aerial target pursuit system reported in the literature.

The system architecture of each pursuer MAV consists of the following modules.

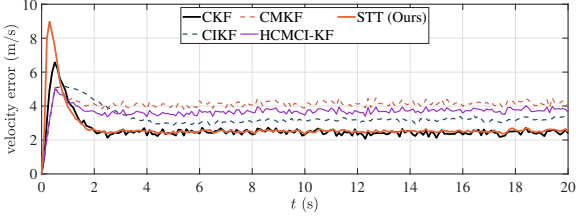
1) The first module is vision-based target detection. Each pursuer MAV has a DJI H20T gimbal camera to sense the target MAV. We trained a YOLO-based detector (YOLOv5s) using a dataset collected by ourselves. The dataset has more than 20,000 images collected in real-world MAV detection scenarios. The reason that we use a YOLO-based detector is because it can achieve a good balance between accuracy and speed as verified by our previous studies [26,27]. The accuracy of the trained detector can reach more than 0.9. The detection frequency is 20 Hz. Although the target detection may not be successful or accurate occasionally, the proposed STT algorithm can well handle these nonidealities.

Once the target has been detected in an image, the bearing vector pointing from the pursuer to the target can be calculated based on its pixel coordinate and the pin-hole camera model [2, Section VII]. We also develop a PI control law to control the gimbal to keep the target at the center of the field-of-view (FOV) of the camera.

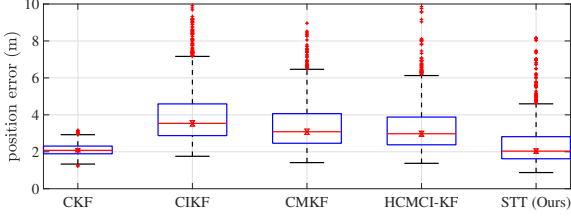
2) The second module is state estimation. Once the bearing vector of the target is obtained from vision, each MAV would use the proposed STT algorithm to fuse the information itself gathers and the information shared by



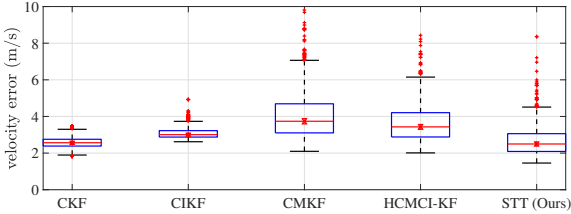
(a) The estimation error of position when the target moves along a circle.



(b) The estimation error of velocity when the target moves along a circle.



(c) The box graph of the mean estimated position errors of square motion.

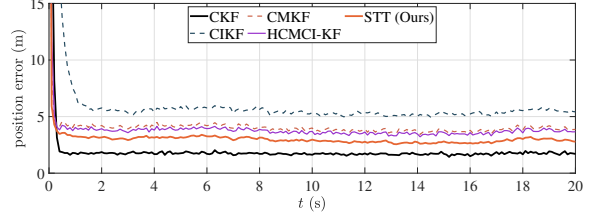


(d) The box graph of the mean estimated velocity errors of square motion.

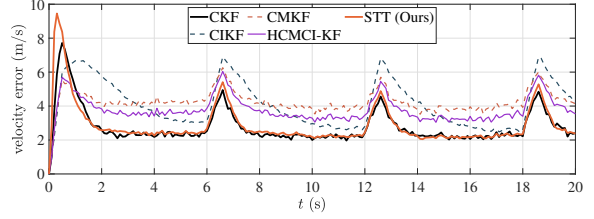
Fig. 2. The simulation results of different estimate algorithms on two different target motion.

its neighbors to estimate the target's motion. The STT algorithm is deployed on the Manifold2G onboard computer, embedded in a robotic operating system (ROS) framework.

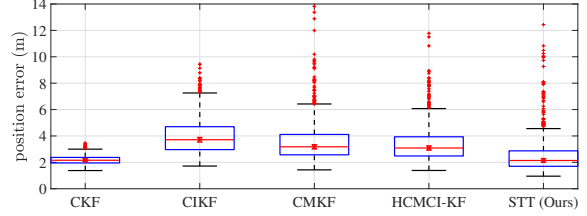
3) The third module is wireless communication. During flight, each pursuer MAV share information with others via wireless communication based on a Zigbee component. The communication frequency of the Zigbee is 30 Hz. Although the bandwidth of Zigbee is not high, it is sufficient for the proposed STT algorithm because STT only requires a small amount of information to be shared among MAVs.



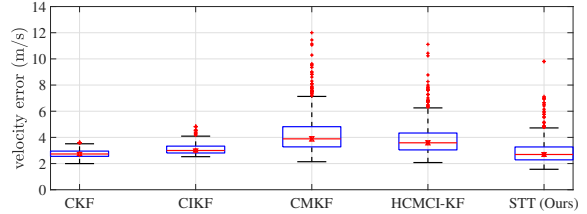
(a) The estimation error of position when the target moves along a square.



(b) The estimation error of velocity when the target moves along a square.



(c) The box graph of the mean estimated position errors of square motion..

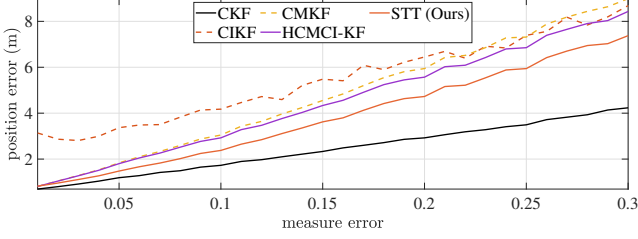


(d) The box graph of the mean estimated position errors of square motion.

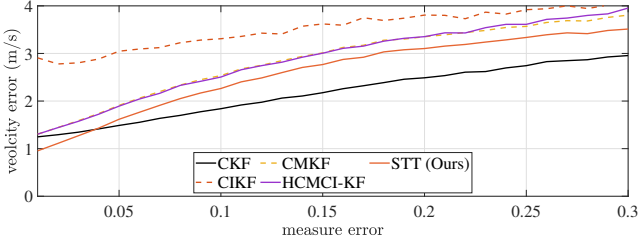
Fig. 3. The simulation results of different estimate algorithms on two different target motion.

4) The fourth module is formation control. Once the target's motion has been estimated, the pursuer MAVs would form a desired formation shape to follow the target. Fig. 5c shows the desired formation shape, where the target MAV is treated as a leader and the pursuer MAVs as followers. In the desired formation shape, the three pursuer MAVs should be distributed evenly on a circle with radius  $r = 7$  m at a vertical height of  $h = 3.5$  m above the target. The horizontal angle between any two pursuer MAVs is 120 degrees. The angle subtended by any two bearing vectors pointing from the pursuers to the target is 90 degrees.

The reason why the desired formation is designed in



(a) The position error with different measurement noises  $\epsilon$ .



(b) The velocity error with different measurement noises  $\epsilon$ .

Fig. 4. The influence of the measure noises on the target state estimation by different estimated algorithms with square motion.

this way is twofold. First, cooperative bearing-only target localization requires certain observability conditions. Loosely speaking, the observability condition requires the pursuers to observe the target from different directions. Otherwise, if the three pursuers observe the target from the same direction (i.e., the bearings are parallel to each other), then it is impossible to localize the target. It has been proven in our previous work [28] that it is an optimal configuration to maximize the observability of the target when the angles between the bearings are 90 degrees. Second, since the camera carried by each pursuer is underneath its body, it is convenient for the pursuer to observe the target if this formation shape can be achieved.

Finally, although we have studied distributed formation control extensively in our previous works [23, 24, 29], we adopted a simple control law here to achieve the desired shape considering that formation control is not the focus in this paper. In particular, once the target's motion has been estimated, the desired position each pursuer can be calculated respectively according to the desired formation shape. A simple way point tracking control law is used to control each pursuer MAV to track the desired position during flight.

The experimental results are shown in Fig. 6. In this experiment, the target MAV is remotely control by a human pilot to fly randomly. The maximum speed and acceleration of the target reach 2.39 m/s and 1.43 m/s<sup>2</sup>, respectively. The trajectories of the pursuer MAVs and the target in 3D space are shown in Fig. 6a. The estimation result of target position and velocity by the STT algorithm are given in Fig. 6b and Fig. 6c, respectively.

Table 3

The mean RMSE of the estimated target state by three pursuer MAVs

	RMSE	position	velocity
MAV1	0.4836	0.2865	
MAV2	0.4706	0.2867	
MAV3	0.4737	0.2818	

As can be seen from the experimental results, the STT algorithm can effectively estimate the target's motion. The overall closed-loop system involving detection, estimation, and control algorithms can work effectively.

## 7 Conclusion

This paper proposed a new algorithm named STT for bearing-only cooperative motion estimation. Unlike the conventional algorithms designed based on DKF, STT is designed based on DRLS. Thanks to the objective function that fully incorporates all the available Information and the triangulation geometric constraints, the STT algorithm generates superior estimation performance than the existing DKFs. It can also achieve comparable performance as the CKF. We also developed a real-world vision-based cooperative aerial target pursuit system to verify the effectiveness of the STT algorithm under practical conditions.

## Appendix

### 7.1 Proof of Lemma 1

There are two terms in the expression of  $\eta_{i,k}$ . The first term  $(\sum_{t=1}^k \lambda_t^{(k)} \mathbf{S}_{i,t}^{(k)})^{-1}$  does not contain any random variables. We thus only need to calculate the expectation of the second term  $\sum_{t=1}^k \lambda_t^{(k)} (\mathbf{y}_{i,t}^{(k)} - \mathbf{S}_{i,t}^{(k)} \mathbf{x}_k)$ .

It follows from the state transition equation (3) that  $\mathbf{x}_{k-1} = \mathbf{A}^{-1} \mathbf{x}_k - \mathbf{A}^{-1} \mathbf{B} \mathbf{w}_{k-1}$ . Then, for any  $t = 1, \dots, k$ , we have  $\mathbf{x}_t = \mathbf{A}^{t-k} \mathbf{x}_k - \sum_{\tau=t}^{k-1} \mathbf{A}^{\tau-k} \mathbf{B} \mathbf{w}_{\tau}$ . Substituting the above equation into the measurement equation (7) gives

$$\begin{aligned} \mathbf{z}_{i,t} &= \mathbf{H}_{i,t} \mathbf{x}_t + \nu_{i,t} \\ &= \mathbf{H}_{i,t} \mathbf{A}^{t-k} \mathbf{x}_k + \nu_{i,t} - \mathbf{H}_{i,t} \sum_{\tau=t}^{k-1} \mathbf{A}^{\tau-k} \mathbf{B} \mathbf{w}_{\tau}, \end{aligned}$$

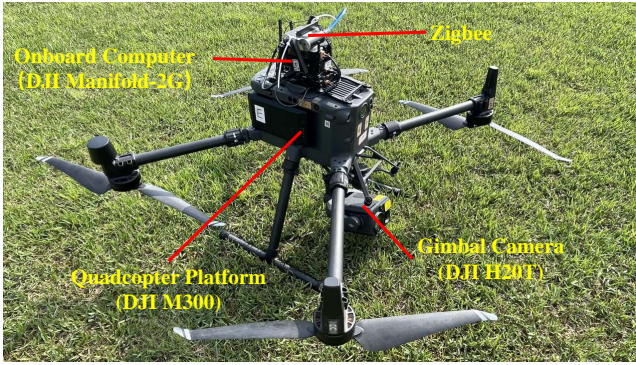
and hence

$$\mathbf{z}_{i,t} - \mathbf{H}_{i,t} \mathbf{A}^{t-k} \mathbf{x}_k = \nu_{i,t} - \mathbf{H}_{i,t} \sum_{\tau=t}^{k-1} \mathbf{A}^{\tau-k} \mathbf{B} \mathbf{w}_{\tau}.$$

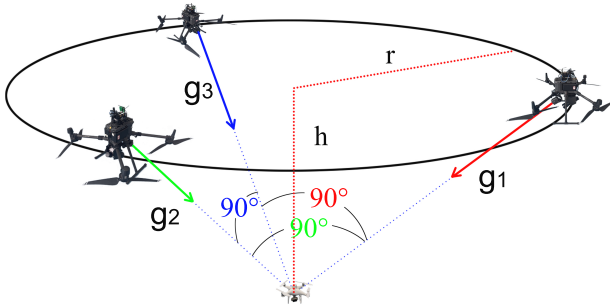




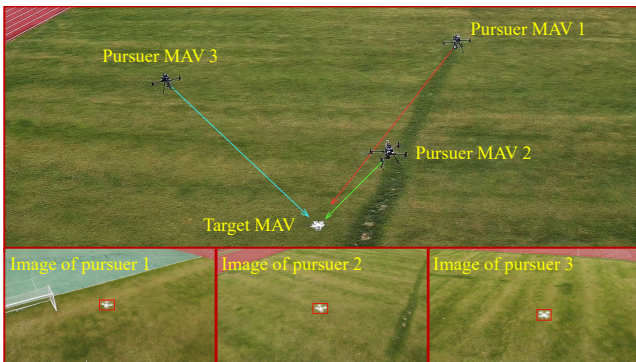
(a) The cooperative pursuer system consists of a target MAV (DJI Phantom 4) and three pursuer MAVs.



(b) The pursuer MAV installs with an onboard computer (DJI Manifold-2G), a zigbee communication, and a gimbal camera (DJI H20T).

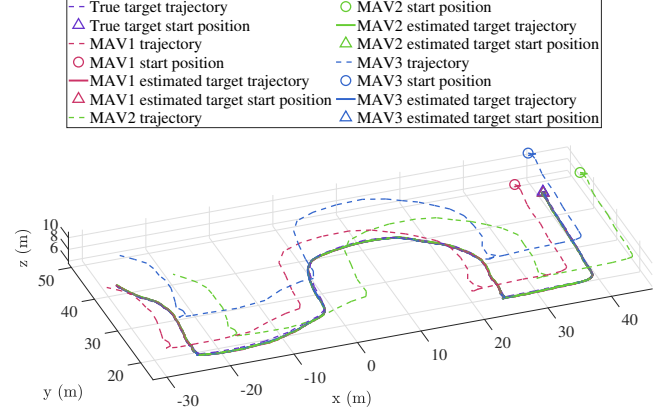


(c) The desired formation shape.

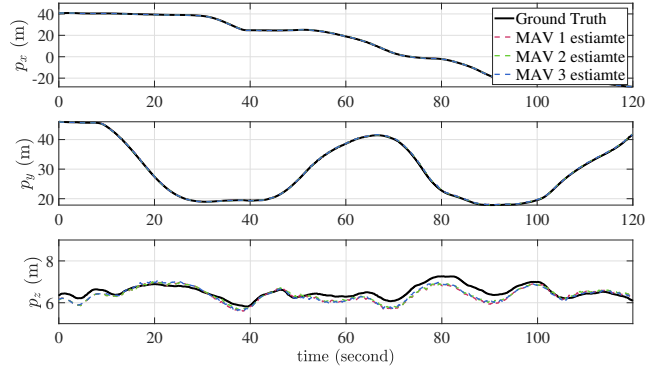


(d) The experimental scenario.

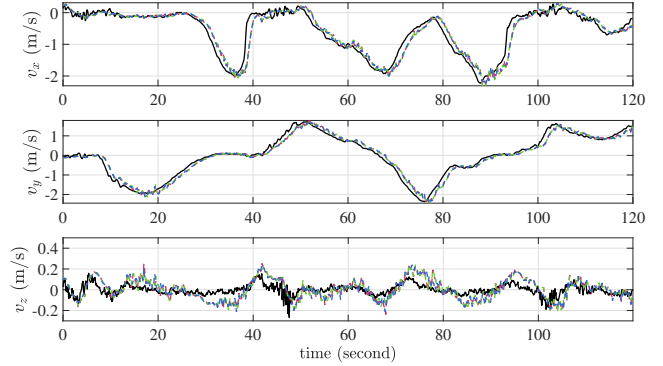
Fig. 5. The purer system consists of a target MAV and three pursuer MAVs as shown in Fig. 5a. Every pursuer MAV installs with an onboard computer, a zigbee communication, and a gimbal camera. When tracing the target MAV, the pursuer system formation shows in Fig. 5c. Fig. 5d gives the exper-



(a) The experimental trajectories.



(b) The ground truth of target position and the estimate target position by three pruser MAVs.



(c) The ground truth of target velocity and the estimate target velocity by three pruser MAVs.

Fig. 6. The Experimental results of tracking an aerial target with three cooperative pursuer MAVs. The symbol  $\Delta$  and  $\bigcirc$  represent the target MAV, and pursuer MAVs starting positions, respectively.

Substituting the above equations into

$$\begin{aligned} & \mathbf{y}_{i,t}^{(k)} - \mathbf{S}_{i,t}^{(k)} \mathbf{x}_k \\ &= (\mathbf{A}^{t-k})^T \left[ \sum_{j \in (i, \mathcal{N}_{i,t})} c\alpha_{ij,t} \mathbf{H}_{j,t}^T \mathbf{R} (\mathbf{z}_{j,t} - \mathbf{H}_{i,t} \mathbf{A}^{t-k} \mathbf{x}_k) \right. \\ & \quad \left. + \sum_{j \in (i, \mathcal{N}_{i,t})} \beta_{ij,t} \hat{\mathbf{x}}_{j,t}^- - \mathbf{A}^{t-k} \mathbf{x}_k \right], \end{aligned} \quad (14)$$

gives

$$\begin{aligned} \mathbf{y}_{i,t}^{(k)} - \mathbf{S}_{i,t}^{(k)} \mathbf{x}_k &= (\mathbf{A}^{t-k})^T \left[ \sum_{j \in (i, \mathcal{N}_{i,t})} c\alpha_{ij,t} \mathbf{H}_{j,t}^T \mathbf{R} \boldsymbol{\nu}_{j,t} \right. \\ &\quad - \sum_{j \in (i, \mathcal{N}_{i,t})} c\alpha_{ij,t} \mathbf{H}_{j,t}^T \mathbf{R} \mathbf{H}_{j,t} \left( \sum_{\tau=t}^{k-1} \mathbf{A}^{\tau-k} \mathbf{B} \mathbf{w}_\tau \right) \\ &\quad \left. + \mathbf{B} \mathbf{w}_{t-1} + \sum_{j \in (i, \mathcal{N}_{i,t})} \beta_{ij,t} \mathbf{A} \boldsymbol{\eta}_{j,t-1} - \sum_{\tau=t}^{k-1} \mathbf{A}^{\tau-k} \mathbf{B} \mathbf{w}_\tau \right]. \end{aligned} \quad (39)$$

Since  $\mathbb{E}[\boldsymbol{\nu}] = 0$  and  $\mathbb{E}[\mathbf{w}] = 0$  by assumption, taking expectation on both sides of the above equation gives

$$\mathbb{E} \left[ \sum_{t=1}^k (\mathbf{y}_{i,t}^{(k)} - \mathbf{S}_{i,t}^{(k)} \mathbf{x}_k) \right] = \mathbb{E}[\bar{\boldsymbol{\eta}}_{i,k}],$$

where  $\bar{\boldsymbol{\eta}}_{i,k}$  is given by (28).

## 7.2 Proof of Lemma 2

The matrix  $\mathbf{S}_{i,t}^{(k)}$  in (21) can be rewritten as

$$\begin{aligned} \mathbf{S}_{i,t}^{(k)} &= c(\mathbf{A}^{t-k})^T \sum_{j \in (i, \mathcal{N}_{i,t})} (\mathbf{H}_{j,t}^T \mathbf{R} \mathbf{H}_{j,t}) \mathbf{A}^{t-k} \\ &\quad + (\mathbf{A}^{t-k})^T \mathbf{A}^{t-k} \\ &= c(\mathbf{A}^{t-k})^T \begin{bmatrix} \frac{1}{\sigma_\nu^2} \sum_{j \in (i \cup \mathcal{N}_{i,t})} \mathbf{P}_{j,t}^T \mathbf{P}_{j,t} & \mathbf{0}_{3 \times 3} \\ \mathbf{0}_{3 \times 3} & \mathbf{0}_{3 \times 3} \end{bmatrix} \mathbf{A}^{t-k} \\ &\quad + (\mathbf{A}^{t-k})^T \mathbf{A}^{t-k} \\ &= \frac{c}{\sigma_\nu^2} \begin{bmatrix} \mathbf{I}_{3 \times 3} & \mathbf{0}_{3 \times 3} \\ (t-k)\Delta t \mathbf{I}_{3 \times 3} & \mathbf{I}_{3 \times 3} \end{bmatrix} \begin{bmatrix} \bar{\mathbf{P}}_{i,t} & \mathbf{0}_{3 \times 3} \\ \mathbf{0}_{3 \times 3} & \mathbf{0}_{3 \times 3} \end{bmatrix} \\ &\quad + \begin{bmatrix} \mathbf{I}_{3 \times 3} & (t-k)\Delta t \mathbf{I}_{3 \times 3} \\ \mathbf{0}_{3 \times 3} & \mathbf{I}_{3 \times 3} \end{bmatrix} + (\mathbf{A}^{t-k})^T \mathbf{A}^{t-k} \\ &= \frac{c}{\sigma_\nu^2} \begin{bmatrix} \bar{\mathbf{P}}_{i,t} & (t-k)\Delta t \bar{\mathbf{P}}_{i,t} \\ (t-k)\Delta t \bar{\mathbf{P}}_{i,t} & (t-k)^2 \Delta t^2 \bar{\mathbf{P}}_{i,t} \end{bmatrix} \\ &\quad + (\mathbf{A}^{t-k})^T \mathbf{A}^{t-k} \\ &= \frac{c}{\sigma_\nu^2} \begin{bmatrix} 1 & (t-k)\Delta t \\ (t-k)\Delta t & (t-k)^2 \Delta t^2 \end{bmatrix} \otimes \bar{\mathbf{P}}_{i,t} \\ &\quad + (\mathbf{A}^{t-k})^T \mathbf{A}^{t-k}. \end{aligned} \quad (40)$$

By defining (32), equation (31) can be obtained from the above equation.

## 7.3 Proof of Lemma 3

For any  $\mathbf{g}_{i,t}$  and  $\mathbf{g}_{j,t}$ , there always exists a rotation matrix  $\mathbf{R}$  so that  $\mathbf{R} \mathbf{g}_{i,t} = \mathbf{g}'_{i,t} = [1, 0, 0]^T$  and  $\mathbf{R} \mathbf{g}_{j,t} = \mathbf{g}'_{j,t} = [\cos \theta_{ij,t}, \sin \theta_{ij,t}, 0]^T$ . The intuition is that  $\mathbf{R}$  aligns  $\mathbf{g}_{i,t}$  with the x-axis and puts  $\mathbf{g}_{j,t}$  in the x-y plane of a new coordinate frame. Then, we have

$$\begin{aligned} \sigma_{\min}(\mathbf{P}_{i,t} + \mathbf{P}_{j,t}) &= \sigma_{\min}[\mathbf{R}(\mathbf{P}_{i,t} + \mathbf{P}_{j,t})\mathbf{R}^T] \\ &= \sigma_{\min}(\mathbf{I}_{3 \times 3} - \mathbf{g}'_{i,t}(\mathbf{g}'_{i,t})^T + \mathbf{I}_{3 \times 3} - \mathbf{g}'_{j,t}(\mathbf{g}'_{j,t})^T) \\ &= \sigma_{\min} \left( \begin{bmatrix} 1 - \cos^2 \theta_{ij,t} & \cos \theta_{ij,t} \sin \theta_{ij,t} & 0 \\ \cos \theta_{ij,t} \sin \theta_{ij,t} & 2 - \sin^2 \theta_{ij,t} & 0 \\ 0 & 0 & 2 \end{bmatrix} \right) \\ &= \sigma_{\min} \left( \begin{bmatrix} 1 - \cos^2 \theta_{ij,t} & \cos \theta_{ij,t} \sin \theta_{ij,t} \\ \cos \theta_{ij,t} \sin \theta_{ij,t} & 2 - \sin^2 \theta_{ij,t} \end{bmatrix} \right). \end{aligned}$$

The singular values of the above two-by-two matrix can be obtained by solving

$$(\sigma - 1 + \cos^2 \theta_{ij,t})(\sigma - 2 + \sin^2 \theta_{ij,t}) - \cos^2 \theta_{ij,t} \sin^2 \theta_{ij,t} = 0.$$

We can solve the roots as  $\sigma = 1 \pm \cos \theta_{ij,t} \geq 0$ . Then the minimum singular value is

$$\sigma_{\min}(\mathbf{P}_{i,t} + \mathbf{P}_{j,t}) = \min\{1 + \cos \theta_{ij,t}, 1 - \cos \theta_{ij,t}\}.$$

When  $\theta_{ij,t} \in [0, \pi/2)$ , we have  $\sigma_{\min}(\mathbf{P}_{i,t} + \mathbf{P}_{j,t}) = 1 - \cos \theta_{ij,t}$ . When  $\theta_{ij,t} \in (\pi/2, \pi)$ , we have  $\sigma_{\min}(\mathbf{P}_{i,t} + \mathbf{P}_{j,t}) = 1 + \cos \theta_{ij,t}$ . Therefore, the minimum singular value can be written in a unified expression:  $\sigma_{\min}(\mathbf{P}_{i,t} + \mathbf{P}_{j,t}) = 1 - |\cos \theta_{ij,t}|$  for any  $\theta_{ij,t} \in [0, \pi)$ .

## 7.4 Proof of Lemma 5

First of all, we have

$$\begin{aligned} \sigma_{\min} \left( \sum_{t=1}^k \lambda_t^{(k)} \mathbf{F}_t^{(k)} \right) &\geq \sigma_{\min} \left( \sum_{t=k-1}^k \lambda_t^{(k)} \mathbf{F}_t^{(k)} \right) \\ &= \sigma_{\min} \left( \lambda_k^{(k)} \mathbf{F}_k^{(k)} + \lambda_{k-1}^{(k)} \mathbf{F}_{k-1}^{(k)} \right). \end{aligned}$$

Since  $\lambda_k^{(k)} \geq \lambda_{k-1}^{(k)}$ , we further have

$$\begin{aligned} \sigma_{\min} \left( \sum_{t=1}^k \lambda_t^{(k)} \mathbf{F}_t^{(k)} \right) &\geq \lambda_{k-1}^{(k)} \sigma_{\min}(\mathbf{F}_k^{(k)} + \mathbf{F}_{k-1}^{(k)}) \\ &= \lambda_{k-1}^{(k)} \sigma_{\min} \left( \begin{bmatrix} 2 & -\Delta t \\ -\Delta t & \Delta t^2 \end{bmatrix} \right). \end{aligned} \quad (41)$$

The singular value of  $(\mathbf{F}_k^{(k)} + \mathbf{F}_{k-1}^{(k)})$  can be obtained by solving  $(x-2)(x-\Delta t^2) - \Delta t^2 = 0$ . The roots are

$$x = \frac{2 + \Delta t^2 \pm \sqrt{4 + \Delta t^4}}{2}. \quad (42)$$

Substituting the minimum root in (42) to (41) gives

$$\begin{aligned} \sigma_{\min} \left( \sum_{t=1}^k c_t \mathbf{F}_t^{(k)} \right) &\geq \lambda_{k-1}^{(k)} \sigma_{\min} (\mathbf{F}_k^{(k)} + \mathbf{F}_{k-1}^{(k)}) \\ &= \lambda_{k-1}^{(k)} \frac{2 + \Delta t^2 - \sqrt{4 + \Delta t^4}}{2}. \end{aligned}$$

The proof is complete.

### 7.5 Proof of Lemma 6

Denote  $\mathbf{P}_0 = \alpha_0(1 - \cos \theta_0) \mathbf{I}_{3 \times 3} \in \mathbb{R}^{3 \times 3}$ . For any  $\mathbf{x}$ , we have  $\mathbf{x}^T (\bar{\mathbf{P}}_{i,t} - \mathbf{P}_0) \mathbf{x} \geq \mathbf{x}^T \bar{\mathbf{P}}_{i,t} \mathbf{x} - \mathbf{x}^T \mathbf{P}_0 \mathbf{x} = \mathbf{x}^T \bar{\mathbf{P}}_{i,t} \mathbf{x} - \alpha_0(1 - \cos \theta_0) \geq \sigma_{\min}(\bar{\mathbf{P}}_{i,t}) - \alpha_0(1 - \cos \theta_0) \geq 0$ , where the last inequality is due to Lemma 4. Therefore, we know that  $(\bar{\mathbf{P}}_{i,t} - \mathbf{P}_0)$  is positive semi-definite. Since  $\mathbf{F}_t^{(k)}$  is also positive semi-definite, we have

$$\sum_{t=1}^k \lambda_t^{(k)} \mathbf{F}_t^{(k)} \otimes (\bar{\mathbf{P}}_{i,t} - \mathbf{P}_0) \geq 0$$

and hence

$$\sum_{t=1}^k \lambda_t^{(k)} \mathbf{F}_t^{(k)} \otimes \bar{\mathbf{P}}_{i,t} \geq \sum_{t=1}^k \lambda_t^{(k)} \mathbf{F}_t^{(k)} \otimes \mathbf{P}_0.$$

It can be further obtained that

$$\begin{aligned} \sigma_{\min} \left( \sum_{t=1}^k \lambda_t^{(k)} \mathbf{F}_t^{(k)} \otimes \bar{\mathbf{P}}_{i,t} \right) &\geq \sigma_{\min} \left( \sum_{t=1}^k \lambda_t^{(k)} \mathbf{F}_t^{(k)} \otimes \mathbf{P}_0 \right) \\ &= \sigma_{\min} \left[ \left( \sum_{t=1}^k \lambda_t^{(k)} \mathbf{F}_t^{(k)} \right) \otimes \mathbf{P}_0 \right] \\ &= \sigma_{\min} \left( \sum_{t=1}^k \lambda_t^{(k)} \mathbf{F}_t^{(k)} \right) \sigma_{\min}(\mathbf{P}_0) \\ &\geq \lambda_{k-1}^{(k)} f(\Delta t) \alpha_0 (1 - \cos \theta_0), \end{aligned}$$

where the last inequality is due to Lemma 5 and  $\sigma_{\min}(\mathbf{P}_0) = \alpha_0(1 - \cos \theta_0)$ . It then follows from (31) that

$$\begin{aligned} \sigma_{\min} \left( \sum_{t=1}^k \lambda_t^{(k)} \mathbf{S}_{i,t}^{(k)} \right) &\geq \sigma_{\min} \left( \sum_{t=1}^k \lambda_t^{(k)} (\mathbf{A}^{t-k})^T \mathbf{A}^{t-k} \right) \\ &\quad + \frac{c}{\sigma_{\nu}^2} \sigma_{\min} \left( \sum_{t=1}^k \lambda_t^{(k)} \mathbf{F}_t^{(k)} \otimes \bar{\mathbf{P}}_{j,t} \right) \\ &\geq \sigma_{\min} \left( \lambda_k^{(k)} (\mathbf{A}^{k-k})^T \mathbf{A}^{k-k} \right) \\ &\quad + \frac{c}{\sigma_{\nu}^2} \lambda_{k-1}^{(k)} f(\Delta t) \alpha_0 (1 - \cos \theta_0) \\ &= \lambda_k^{(k)} + \frac{c}{\sigma_{\nu}^2} \lambda_{k-1}^{(k)} f(\Delta t) \alpha_0 (1 - \cos \theta_0). \quad (43) \end{aligned}$$

If

$$\begin{aligned} c &\geq \frac{(1 - \lambda_k^{(k)}) \sigma_{\nu}^2}{\lambda_{k-1}^{(k)} f(\Delta t) \alpha_0 (1 - \cos \theta_0)} \\ &= \frac{(\|\mathbf{A}\|(1 + \gamma_1) - 1) \|\mathbf{A}\| (1 + \gamma_1) \sigma_{\nu}^2}{\gamma_2 f(\Delta t) \alpha_0 (1 - \cos \theta_0)}, \end{aligned}$$

then substituting  $c$ , given in (36), into (43) yields

$$\begin{aligned} \sigma_{\min} \left( \sum_{t=1}^k \lambda_t^{(k)} \mathbf{S}_{i,t}^{(k)} \right) &\geq \lambda_k^{(k)} \\ &\quad + \frac{c}{\sigma_{\nu}^2} \lambda_{k-1}^{(k)} f(\Delta t) \alpha_0 (1 - \cos \theta_0) \\ &\geq 1. \end{aligned}$$

The proof is complete.

### 7.6 Algorithms for comparison

For a quick reference, we list the algorithms that are used to compare with our proposed one.

#### 7.6.1 Centralized Kalman Filter (CKF)

CKF is a baseline for evaluating the performance of distributed estimation algorithms. It assumes there exist a central node that can obtain all the measurements from all the observers. The CKF algorithm in the central node is given as follows.

**Prediction:**

$$\begin{aligned} \hat{\mathbf{x}}_{k+1}^- &= \mathbf{A} \hat{\mathbf{x}}_k, \\ \hat{\mathbf{P}}_{k+1}^- &= \mathbf{A} \hat{\mathbf{P}}_k \mathbf{A}^T + \mathbf{B} \mathbf{Q} \mathbf{B}^T, \end{aligned}$$



**Measurement:**

$$\begin{aligned} \mathbf{y}_{k+1} &= \sum_{i \in \mathcal{V}} \mathbf{H}_{i,k+1}^T \mathbf{R}_i^{-1} \mathbf{z}_{i,k+1}, \\ \mathbf{S}_{k+1} &= \sum_{i \in \mathcal{V}} \mathbf{H}_{i,k+1}^T \mathbf{R}_i^{-1} \mathbf{H}_{i,k+1}, \end{aligned}$$

**Correction:**

$$\begin{aligned} \mathbf{K}_{k+1} &= \left( \left( \hat{\mathbf{P}}_{k+1}^- \right)^{-1} + \mathbf{S}_{k+1} \right)^{-1}, \\ \hat{\mathbf{x}}_{k+1} &= \hat{\mathbf{x}}_{k+1}^- + \mathbf{K}_{k+1} (\mathbf{y}_{k+1} - \mathbf{S}_{k+1} \hat{\mathbf{x}}_{k+1}^-), \\ \hat{\mathbf{P}}_{k+1} &= (\mathbf{I}_{6 \times 6} - \mathbf{K}_{k+1} \mathbf{S}_{k+1}) \hat{\mathbf{P}}_{k+1}^-. \end{aligned}$$

### 7.6.2 Consensus Measurement Kalman Filter (CMKF)

This method assumes that within a communication network, each node can obtain the *measurements* of its neighbors. For the  $i$ th observer, the CMKF algorithm is as follows.

**Prediction:**

$$\begin{aligned} \hat{\mathbf{x}}_{i,k+1}^- &= \mathbf{A} \hat{\mathbf{x}}_{i,k}, \\ \hat{\mathbf{P}}_{i,k+1}^- &= \mathbf{A} \hat{\mathbf{P}}_{i,k} \mathbf{A}^T + \mathbf{B} \mathbf{Q} \mathbf{B}^T, \end{aligned}$$

**Consensus on measurement:**

$$\begin{aligned} \mathbf{y}_{i,k+1} &= \sum_{j \in (i \cup \mathcal{N}_{i,k+1})} \beta_{ij} \mathbf{H}_{j,k+1}^T \mathbf{R}_j^{-1} \mathbf{z}_{j,k+1}, \\ \mathbf{S}_{i,k+1} &= \sum_{j \in (i \cup \mathcal{N}_{i,k+1})} \beta_{ij} \mathbf{H}_{j,k+1}^T \mathbf{R}_j^{-1} \mathbf{H}_{j,k+1}, \end{aligned}$$

**Correction:**

$$\begin{aligned} \mathbf{K}_{i,k+1} &= \left( \left( \hat{\mathbf{P}}_{i,k+1}^- \right)^{-1} + \mathbf{S}_{i,k+1} \right)^{-1}, \\ \hat{\mathbf{x}}_{i,k+1} &= \hat{\mathbf{x}}_{i,k+1}^- + \mathbf{K}_{i,k+1} (\mathbf{y}_{i,k+1} - \mathbf{S}_{i,k+1} \hat{\mathbf{x}}_{i,k+1}^-), \\ \hat{\mathbf{P}}_{i,k+1} &= (\mathbf{I}_{6 \times 6} - \mathbf{K}_{i,k+1} \mathbf{S}_{i,k+1}) \hat{\mathbf{P}}_{i,k+1}^-. \end{aligned}$$

### 7.6.3 Consensus Information Kalman Filter (CIKF)

The CIKF algorithm [15] is proposed for realizing the consensus of all the estimates in a distributed network. The formal CIKF method consists of two components: a standard Kalman estimator and a consensus algorithm. For the  $i$ th observer, the algorithm is as follows.

**Prediction:**

$$\begin{aligned} \hat{\mathbf{x}}_{i,k+1}^- &= \mathbf{A} \hat{\mathbf{x}}_{i,k}, \\ \hat{\mathbf{P}}_{i,k+1}^- &= \mathbf{A} \hat{\mathbf{P}}_{i,k} \mathbf{A}^T + \mathbf{B} \mathbf{Q} \mathbf{B}^T, \end{aligned}$$

**Correction:**

$$\begin{aligned} \mathbf{K}_{i,k+1} &= \hat{\mathbf{P}}_{i,k+1}^- \mathbf{H}_{i,k+1}^T \left( \mathbf{R}_i + \mathbf{H}_{i,k+1} \hat{\mathbf{P}}_{i,k+1}^- \mathbf{H}_{i,k+1}^T \right)^{-1}, \\ \hat{\mathbf{x}}_{i,k+1}^{(0)} &= \hat{\mathbf{x}}_{i,k+1}^- + \mathbf{K}_{i,k+1} \left( \mathbf{z}_{i,k+1} - \mathbf{H}_{i,k+1} \hat{\mathbf{x}}_{i,k+1}^- \right), \\ \hat{\mathbf{P}}_{i,k+1}^{(0)} &= (\mathbf{I}_{3 \times 3} - \mathbf{K}_{i,k+1} \mathbf{H}_{i,k+1}) \hat{\mathbf{P}}_{i,k+1}^-, \end{aligned}$$

**Consensus on information:**

for  $l = 1, 2, \dots, L$

$$\begin{aligned} \hat{\mathbf{x}}_{i,k+1}^{(l)} &= \hat{\mathbf{x}}_{i,k+1}^{(l-1)} + \sum_{j \in \mathcal{N}_{i,k+1}} \beta_{ij} \left( \hat{\mathbf{x}}_{j,k+1}^{(l-1)} - \hat{\mathbf{x}}_{i,k+1}^{(l-1)} \right), \\ \hat{\mathbf{P}}_{i,k+1}^{(l)} &= \hat{\mathbf{P}}_{i,k+1}^{(l-1)} + \sum_{j \in \mathcal{N}_{i,k+1}} \beta_{ij} \left( \hat{\mathbf{P}}_{j,k+1}^{(l-1)} - \hat{\mathbf{P}}_{i,k+1}^{(l-1)} \right), \end{aligned}$$

end

$$\begin{aligned} \hat{\mathbf{x}}_{i,k+1} &= \hat{\mathbf{x}}_{i,k+1}^{(L)}, \\ \hat{\mathbf{P}}_{i,k+1} &= \hat{\mathbf{P}}_{i,k+1}^{(L)}. \end{aligned}$$

### 7.6.4 Hybrid Consensus on Measurement and Information Kalman Filter (HCMCI-KF)

The HCMCI-KF algorithm [17] can be viewed as a combination of CMKF and CIKF. It also achieves the best performance among the existing DKF algorithms as verified by our simulation. The algorithm is as follows.

**Prediction:**

$$\begin{aligned} \hat{\mathbf{x}}_{i,k+1}^- &= \mathbf{A} \hat{\mathbf{x}}_{i,k}, \\ \hat{\mathbf{\Omega}}_{i,k+1}^{(0)-} &= \mathbf{W} - \mathbf{W} \mathbf{A} \left( \hat{\mathbf{\Omega}}_{i,k} + \mathbf{A}^T \mathbf{W} \mathbf{A} \right)^{-1} \mathbf{A}^T \mathbf{W}, \\ \hat{\mathbf{q}}_{i,k+1}^{(0)-} &= \left( \hat{\mathbf{\Omega}}_{i,k+1}^- \right)^{-1} \hat{\mathbf{x}}_{i,k+1}^-, \end{aligned}$$

**Consensus on measurements and information:**

$$\begin{aligned} \mathbf{S}_{i,k+1}^{(0)} &= \mathbf{H}_{i,k+1}^T \mathbf{R}_i^{-1} \mathbf{H}_{i,k+1}, \\ \mathbf{y}_{i,k+1}^{(0)} &= \mathbf{H}_{i,k+1}^T \mathbf{R}_i^{-1} \mathbf{z}_{i,k+1}, \end{aligned}$$

for  $l = 1, 2, \dots, L$

$$\begin{aligned} \mathbf{y}_{i,k+1}^{(l+1)} &= \sum_{j \in (i \cup \mathcal{N}_{i,k+1})} \beta_{ij} \mathbf{y}_{j,k+1}^{(l)}, \\ \mathbf{S}_{i,k+1}^{(l+1)} &= \sum_{j \in (i \cup \mathcal{N}_{i,k+1})} \beta_{ij} \mathbf{S}_{j,k+1}^{(l)}, \\ \hat{\mathbf{q}}_{i,k+1}^{(l+1)-} &= \sum_{j \in (i \cup \mathcal{N}_{i,k+1})} \beta_{ij} \hat{\mathbf{q}}_{j,k+1}^{(l)-}, \\ \hat{\mathbf{\Omega}}_{i,k+1}^{(l+1)-} &= \sum_{j \in (i \cup \mathcal{N}_{i,k+1})} \beta_{ij} \hat{\mathbf{\Omega}}_{j,k+1}^{(l)-}, \end{aligned}$$

end

**Correction:**

$$\begin{aligned} \hat{\mathbf{q}}_{i,k+1} &= \hat{\mathbf{q}}_{i,k+1}^{(L)-} + \omega_i \mathbf{y}_{i,k+1}^{(L)}, \\ \hat{\mathbf{\Omega}}_{i,k+1} &= \hat{\mathbf{\Omega}}_{i,k+1}^{(L)-} + \omega_i \mathbf{S}_{i,k+1}^{(L)}, \\ \hat{\mathbf{x}}_{i,k+1} &= \hat{\mathbf{\Omega}}_{i,k+1} \hat{\mathbf{q}}_{i,k+1}. \end{aligned}$$

In this algorithm,  $\mathbf{W}$  and  $\hat{\mathbf{\Omega}}_{i,k}$  are defined as

$$\begin{aligned} \mathbf{W} &= \mathbf{Q}^{-1}, \\ \hat{\mathbf{\Omega}}_{i,k} &= \hat{\mathbf{P}}_{i,k}^{-1}, \end{aligned}$$

where  $\mathbf{Q}$  is the noise information matrix, and  $\hat{\mathbf{P}}_{i,k}$  is the covariance matrix.

In summary, CKF needs a central node for the collection of all the measurements. It therefore can achieve better estimation performance than the distributed ones. CMKF can only achieve local optimal estimation based on local measurements. CIKF uses the consensus algorithm after the correction step and achieves global consensus, but the convergence speed is slower than CMKF in general. Since HCMCI-KF can be viewed as a combination of CMKF and CIKF, it can achieve better performance than CMKF and CIKF in general as shown in our simulation.

## References

- [1] C. H. Brighton and G. K. Taylor, "Hawks steer attacks using a guidance system tuned for close pursuit of erratically manoeuvring targets," *Nature Communications*, vol. 10, no. 1, p. 2462, 2019.
- [2] J. Li, Z. Ning, S. He, C.-H. Lee, and S. Zhao, "Three-dimensional bearing-only target following via observability-enhanced helical guidance," *IEEE Transactions on Robotics*, 2022.
- [3] T.-H. Kim and T. Sugie, "Cooperative control for target-capturing task based on a cyclic pursuit strategy," *Automatica*, vol. 43, no. 8, pp. 1426–1431, 2007.
- [4] L. Ma and N. Hovakimyan, "Vision-based cyclic pursuit for cooperative target tracking," *Journal of Guidance, Control, and Dynamics*, vol. 36, no. 2, pp. 617–622, 2013.
- [5] V. R. Makkapati and P. Tsiotras, "Optimal evading strategies and task allocation in multi-player pursuit–evasion problems," *Dynamic Games and Applications*, vol. 9, pp. 1168–1187, 2019.
- [6] F. Borra, L. Biferale, M. Cencini, and A. Celani, "Reinforcement learning for pursuit and evasion of microswimmers at low reynolds number," *Physical Review Fluids*, vol. 7, no. 2, p. 023103, 2022.
- [7] M. Vrba, D. Heřt, and M. Saska, "Onboard marker-less detection and localization of non-cooperating drones for their safe interception by an autonomous aerial system," *IEEE Robotics and Automation Letters*, vol. 4, no. 4, pp. 3402–3409, 2019.
- [8] X. Lin, T. Kirubarajan, Y. Bar-Shalom, and S. Maskell, "Comparison of EKF, pseudomeasurement, and particle filters for a bearing-only target tracking problem," in *Signal and Data Processing of Small Targets*, vol. 4728, 2002, pp. 240–250.
- [9] K. Doğançay, "Bearings-only target localization using total least squares," *Signal Processing*, vol. 85, no. 9, pp. 1695–1710, 2005.
- [10] D. E. George and A. Unnikrishnan, "On the divergence of information filter for multi sensors fusion," *Information Fusion*, vol. 27, pp. 76–84, 2016.
- [11] S. Xu, K. Doğançay, and H. Hmam, "Distributed pseudolinear estimation and UAV path optimization for 3D AOA target tracking," *Signal Processing*, vol. 133, pp. 64–78, 2017.
- [12] N. H. Nguyen and K. Doğançay, "Instrumental variable based Kalman filter algorithm for three-dimensional AOA target tracking," *IEEE Signal Processing Letters*, vol. 25, no. 10, pp. 1605–1609, 2018.
- [13] H. Jiang, X. Wang, Y. Deng, and Y. Zhang, "Event-triggered distributed bias-compensated pseudolinear information filter for bearings-only tracking under measurement uncertainty," *IEEE Sensors Journal*, 2023.
- [14] R. Olfati-Saber and J. S. Shamma, "Consensus filters for sensor networks and distributed sensor fusion," in *Proceedings of the 44th IEEE Conference on Decision and Control*. IEEE, 2005, pp. 6698–6703.
- [15] R. Olfati-Saber, "Kalman-consensus filter: Optimality, stability, and performance," in *Proceedings of the 48th IEEE Conference on Decision and Control (CDC) held jointly with the 28th Chinese Control Conference*, pp. 7036–7042.
- [16] G. Battistelli and L. Chisci, "Kullback–Leibler average, consensus on probability densities, and distributed state estimation with guaranteed stability," *Automatica*, vol. 50, no. 3, pp. 707–718, 2014.
- [17] G. Battistelli, L. Chisci, G. Mugnai, A. Farina, and A. Graziano, "Consensus-based linear and nonlinear filtering," *IEEE Transactions on Automatic Control*, vol. 60, no. 5, pp. 1410–1415, 2014.
- [18] R. I. Hartley and P. Sturm, "Triangulation," *Computer vision and image understanding*, vol. 68, no. 2, pp. 146–157, 1997.
- [19] A. H. Sayed and T. Kailath, "A state-space approach to adaptive RLS filtering," *IEEE Signal Processing Magazine*, vol. 11, no. 3, pp. 18–60, 1994.
- [20] F. S. Cattivelli, C. G. Lopes, and A. H. Sayed, "Diffusion recursive least-squares for distributed estimation over adaptive networks," *IEEE Transactions on Signal Processing*, vol. 56, no. 5, pp. 1865–1877, 2008.

- [21] P. Di Lorenzo and G. Scutari, "Next: In-network nonconvex optimization," *IEEE Transactions on Signal and Information Processing over Networks*, vol. 2, no. 2, pp. 120–136, 2016.
- [22] R. Arablouei, K. Doğançay, S. Werner, and Y.-F. Huang, "Adaptive distributed estimation based on recursive least-squares and partial diffusion," *IEEE Transactions on Signal Processing*, vol. 62, no. 14, pp. 3510–3522, 2014.
- [23] S. Zhao and D. Zelazo, "Bearing rigidity and almost global bearing-only formation stabilization," *IEEE Transactions on Automatic Control*, vol. 61, no. 5, pp. 1255–1268, 2015.
- [24] S. Zhao, Z. Li, and Z. Ding, "Bearing-only formation tracking control of multiagent systems," *IEEE Transactions on Automatic Control*, vol. 64, no. 11, pp. 4541–4554, 2019.
- [25] H. V. Henderson and S. R. Searle, "On deriving the inverse of a sum of matrices," *SIAM Review*, vol. 23, no. 1, pp. 53–60, 1981.
- [26] Y. Zheng, Z. Chen, D. Lv, Z. Li, Z. Lan, and S. Zhao, "Air-to-air visual detection of micro-UAVs: An experimental evaluation of deep learning," *IEEE Robotics and Automation Letters*, vol. 6, no. 2, pp. 1020–1027, 2021.
- [27] Y. Zheng, C. Zheng, X. Zhang, F. Chen, Z. Chen, and S. Zhao, "Detection, localization, and tracking of multiple mavs with panoramic stereo camera networks," *IEEE Transactions on Automation Science and Engineering*, 2022.
- [28] S. Zhao, B. M. Chen, and T. H. Lee, "Optimal sensor placement for target localisation and tracking in 2D and 3D," *International Journal of Control*, vol. 86, no. 10, pp. 1687–1704, 2013.
- [29] S. Zhao and D. Zelazo, "Localizability and distributed protocols for bearing-based network localization in arbitrary dimensions," *Automatica*, vol. 69, pp. 334–341, 2016.